AD-A246 408

US ARMY
LABORATORY COMMAND
MATERIALS TECHNOLOGY LABORATORY

MTL TR 92-7

DEVELOPMENT OF TUNGSTEN BASED COMPOSITES
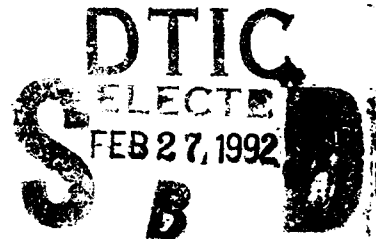
February 1992

MURRAY KORNHAUSER

3C Systems, Inc.
620 Argyle Road
Wynnewood, PA 19096

ROBERT J. DOWDING
U.S. Army Materials Technology Laboratory
Materials Producibility Branch

DTIC
ELECTE
FEB 27, 1992
S B D

FINAL REPORT   Contract DAAL04-91-C-0012

Prepared for

U.S. ARMY MATERIALS TECHNOLOGY LABORATORY
Watertown, Massachusetts 02172-0001

92-04673

92 2 24 060

The findings in this report are not to be construed as an official Department of the Army position, unless so designated by other authorized documents.

Mention of any trade names or manufacturers in this report shall not be construed as advertising nor as an official indorsement or approval of such products or companies by the United States Government.

REPORT DOCUMENTATION PAGE		READ INSTRUCTIONS BEFORE COMPLETING FORM
1. REPORT NUMBER MTL TR 92-7	2. GOVT ACCESSION NO.	3. RECIPIENT'S CATALOG NUMBER
4. TITLE *(and Subtitle)* DEVELOPMENT OF TUNGSTEN BASED COMPOSITES		5. TYPE OF REPORT & PERIOD COVERED Final Report-February 1991 – October 1991
		6. PERFORMING ORG. REPORT NUMBER
7. AUTHOR(s) Murray Kornhauser and Robert J. Dowding*		8. CONTRACT OR GRANT NUMBER(s) DAAL04-91-C-0012
9. PERFORMING ORGANIZATION NAME AND ADDRESS 3C Systems, Inc. 620 Argyle Road Wynnewood, PA 19096		10. PROGRAM ELEMENT, PROJECT, TASK AREA & WORK UNIT NUMBERS
11. CONTROLLING OFFICE NAME AND ADDRESS U.S. Army Materials Technology Laboratory ATTN: SLCMT-PR Watertown, MA 02172-0001		12. REPORT DATE February 1992
		13. NUMBER OF PAGES 86
14. MONITORING AGENCY NAME & ADDRESS *(if different from Controlling Office)*		15. SECURITY CLASS. *(of this report)* Unclassified
		15a. DECLASSIFICATION/DOWNGRADING SCHEDULE

16. DISTRIBUTION STATEMENT *(of this Report)*

Approved for public release; distribution unlimited.

17. DISTRIBUTION STATEMENT *(of the abstract entered in Block 20, if different from Report)*

18. SUPPLEMENTARY NOTES

*MTL, Materials Producibility Branch
Robert J. Dowding, COR

19. KEY WORDS *(Continue on reverse side if necessary and identify by block number)*

Tungsten alloys	Adiabatic shear
Tungsten composites	High strain rate testing
Dynamic tests	Hopkinson bar testing

20. ABSTRACT *(Continue on reverse side if necessary and identify by block number)*

(SEE REVERSE SIDE)

DD FORM 1473 EDITION OF 1 NOV 65 IS OBSOLETE
1 JAN 73

Block No. 20

ABSTRACT

    The objectives of this Phase I SBIR Program were to develop the test facility for very high strain rate shear testing of composite tungsten materials for use in kinetic energy (KE) penetrators, to test some composites prepared by liquid phase sintering and by the HIP process, and to determine whether the test samples exhibit evidence of favorable KE properties. An electromagnetic stress wave generator, with its output augmented with a conical Hopkinson bar, was used to drive a half-inch diameter punch through tungsten composite samples 1/16 inch thick and one-inch diameter. Initial strain rate on impact was up to 2.4×10^7 sec^{-1}, decreasing as the punch was decelerated by the test sample's resistance. Metallographic examinations were made; however, it is too early to report on promising trends. Phase II would include penetrator performance testing on target.

Accession For

NTIS GRA&I   ☑
DTIC TAB   ☐
Unannounced   ☐
Justification_____

By_____
Distribution/
    Availability Codes

Dist | Avail and/or Special

A/1

DTIC
COPY
INSPECTED
4

TABLE OF CONTENTS

LIST OF FIGURES

LIST OF TABLES

1. INTRODUCTION & SUMMARY

This is the Final Report on a Phase I SBIR Program entitled "Development of Tungsten Based Composites", Contract No. DAAL04-91-C-0012, performed for the U.S. Army Materials Technology Laboratory in Watertown, Massachusetts.

The ultimate objective of this research is to develop high density tungsten composite materials that will exhibit behavior such as adiabatic shear banding that will enhance kinetic energy penetrator performance by maximizing penetration depth. As described by Magness and Farrand, the role of adiabatic shear is to permit the penetrator nose to shed material from its periphery rather than to mushroom, thereby minimizing the area of loading on the penetrator and minimizing the deceleration of the penetrator during the penetration process. The "self sharpening" penetrator penetrates deeper into monolithic targets and penetrates through individual plates with less velocity loss.

The immediate objectives of the Phase I program were to develop the test facility and methodology for very-high strain rate shear testing of promising tungsten composites prepared by liquid phase sintering and by hot isostatic pressing (HIP), to test some candidate materials, and to determine whether these test samples exhibit evidence of properties favorable for KE penetrators. Expansion of this program to include other materials, to include tensile stress-strain testing at very-high strain rates in the laboratory, and to include quarter scale penetrator performance testing on the target, would be considered for Phase II.

An electromagnetic stress wave generator, with its output augmented with a conical Hopkinson bar, was used to drive a half-inch diameter punch through tungsten composite samples 1/16 inch

thick and one-inch diameter. The stress wave generator, with a design limit of approximately 10 kilovolts input, was employed only in its lower range, mainly at 2 KV and 3 KV, plus a few shots up to 5 KV. In this low range, the strain rate was of the order of 10^6 sec^{-1}, depending on an impact velocity of the order of 100 ft/sec and the punch's diametral clearance of 0.0006 inches.

Two kinds of punch were employed; a flat punch and a punch with a tilted or slant face. This latter approach to shear testing looks very promising, since it makes it possible to vary the strain rate within a single test and with a single material sample. The slant punch leading edge starts shearing through the test disk at full punch velocity, while subsequent shearing by the trailing portions of the punch is accomplished at lower velocities since the punch is being slowed down by the shearing resistance of the test sample. Therefore, different parts of the disk are being sheared out at different strain rates. Note that measurements of punch deceleration will be required to determine strain rate variations during the punching process. It must also be noted that some tensile strains may be expected, rather than pure shear strains.

Another test methodology partly developed in Phase I was to heat the test specimen enough to obtain phase transitions (see Appendix A, for example) of the materials used to coat the tungsten particles, thereby simulating the on-target heating generated by the impact stress waves. Although the sample's temperature was not measured with precisior and it was allowed to vary during the test (both of which deficiencies can be corrected with a minimum of further development), this approach to high strain rate testing at elevated temperatures appears entirely feasible.

Five HIPed materials prepared by Industrial Materials Technology, Inc. of Andover, Massachusetts were tested, as well as samples of a GTE-provided tungsten composite. Examination of the

microstucture of these samples after high strain rate shear testing indicated material responses that could affect the performance of kinetic energy penetrators. However, because of the small number of material composition and processing variations explored in Phase I, it is too early to report on promising trends in development of tungsten composites.

2. MATERIAL SELECTION

In Reference 2, Dowding presents an up-to-date review of the U.S. Army research into tungsten heavy alloys (WHA) being conducted by the Materials Technology Laboratory. Tungsten particles embedded in matrices of nickel, copper, iron, etc. have been sintered (liquid phase sintering), heat treated and cold worked. Tungsten powder materials coated with nickel, iron, and/or cobalt have been prepared by chemical vapor deposition (CVD) and consolidated by the Ceracon process (Ceracon Corp., Sacramento, CA) or by HIPing. The samples tested in Phase I were prepared, by this latter process, by Industrial Materials Technology, Inc. of Andover, Massachusetts. See Appendix A.

It is important to address the question of how the stress-wave-generated heating of the penetrator will affect the properties of the tungsten and its alloying elements. Figure 1 contains plots of stress wave pressures and associated temperature increases (taken from Reference 3) when tungsten impacts steel at high velocities. At the 1.5 km/sec impact velocity used in quarter-scale testing of penetrators, the shock-induced temperature increases are less than 200 degrees C. However, as operational impact velocities for KE penetrators increase, the steeply rising temperature curve in Figure 1 will enter regimes where there will

Fig. 1 Pressure and Temperature Rise When Tungsten Strikes Steel
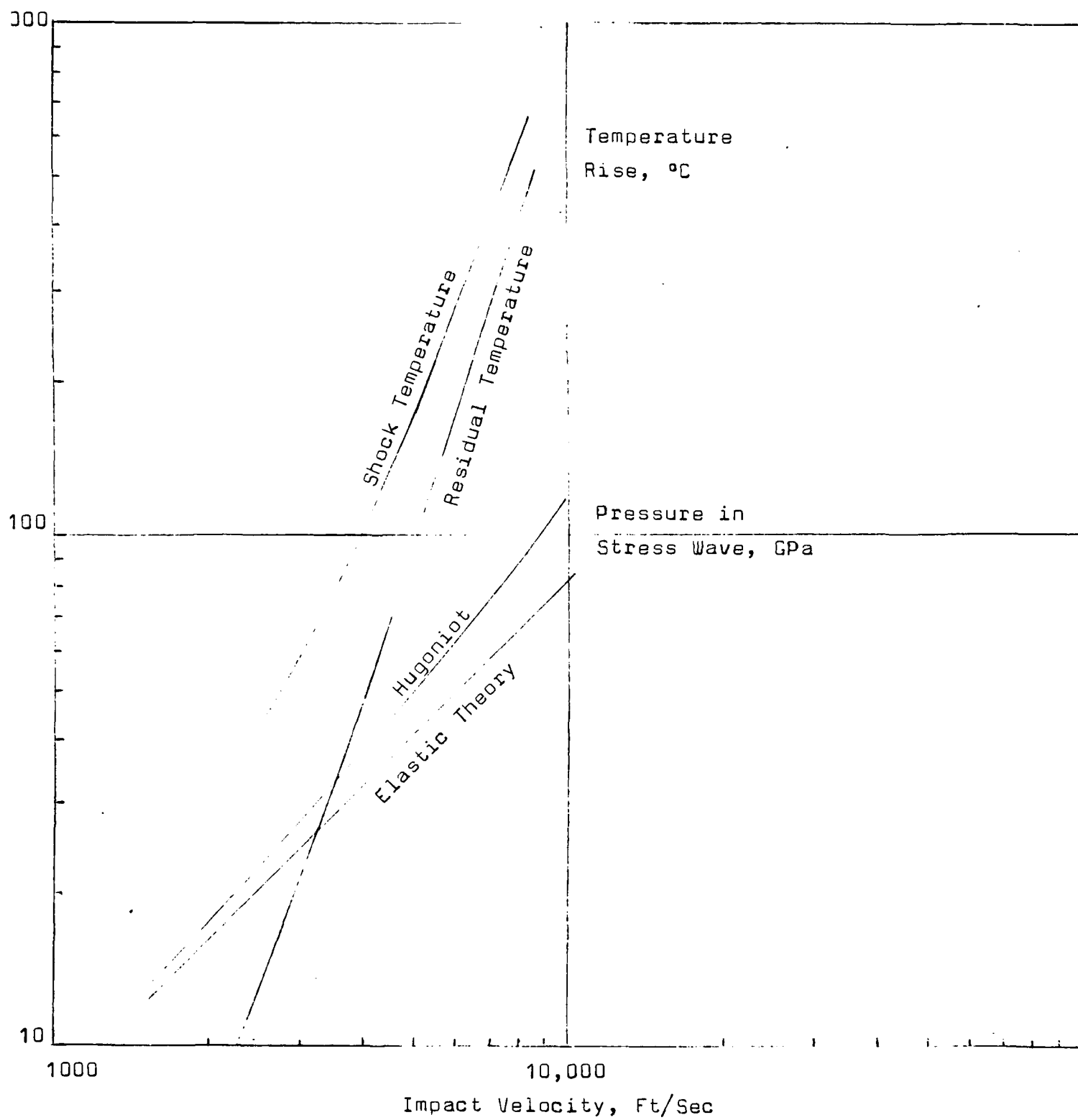
be phase transitions of the alloying elements. For this reason, titanium was used as the alloying element in three of the test samples (see Appendix A for Ti-W phase diagrams). For this test series, titanium was included as 30 percent, 40 percent, and 50 percent by volume. In addition to shock wave heat generated by bulk compression of the tungsten, there will likely be heat generated at the matrix interfaces as they are deformed. Partition of this heat between the tungsten particles and the matrix materials will depend on their relative thermal diffusivities. Material selection using thermal diffusivity as a criterion was not done in Phase I, but it bears study in future work.

Additional HIPed materials were coated tungsten powder with a composition of 95.4% W-3.0% Ni-1.6% Fe and a zirconium foil (2 mils) laminate. In addition, a GTE tungsten alloy (tungsten blended with 8% nickel and 2% iron) was selected as a baseline material for purposes of comparison.

3. DEVELOPMENT OF TEST FACILITY

3.1 Electromagnetic Stress Wave Generator

An electromagnetic stress wave generator was designed under U.S. Army Contract DAAA21-85-C-0299, Picatinny Arsenal, (Reference 4), for use in shock testing (G loading, as opposed to electrical shock) ordnance components up to 200,000G. The electrical design is reported in Reference 4. The stress wave generator consists essentially of a capacitor bank that dumps its stored energy suddenly into a flat pancake coil, against the surface of which rests either an aluminum carriage (in the case of the shock tester, to hold the device being accelerated) or the end of a Hopkinson bar, for dynamic stress testing.

Dynamic shear testing is accomplished by accelerating a steel punch from the end of a Hopkinson bar to strike a die holding the test sample. The overall assembly is shown in Figure 2. If the punch face is initially in contact with the test sample, its shearing velocity will start at zero and increase to its full value within approximately 75 microseconds (using the currently operational electromagnetic coil). Figure 3 contains plots of velocity versus time for a punch that is integral with the end of the Hopkinson bar, indicating a full cycle time of 150 microseconds. However, if the punch is free to be launched from the bar's end, it will lose contact with the bar in approximately 75 microseconds. Since the punch simply rests against the end of the Hopkinson bar, it is employed with enough gap between its punching face and the test sample in order to develop its full velocity potential by the time it contacts the test sample. The strain rate in shear testing depends on shearing velocity v and punch-die clearance, x, as follows:

$$\dot{\epsilon} = d\epsilon/dt = v/x \qquad\qquad (1)$$

To achieve high strain rates with practical punch clearances, therefore, it is desired to maximize v. Punch velocity is proportional to the impulse delivered at the end of the Hopkinson bar, which is proportional to the impulse delivered by the electromagnetic coil. Impulse is equal to pressure times loading duration, for a given loading area. Pressure is proportional to N^2V^2C/L and loading duration is proportional to $(LC)^{\frac{1}{2}}$; therefore impulse is proportional to the following:

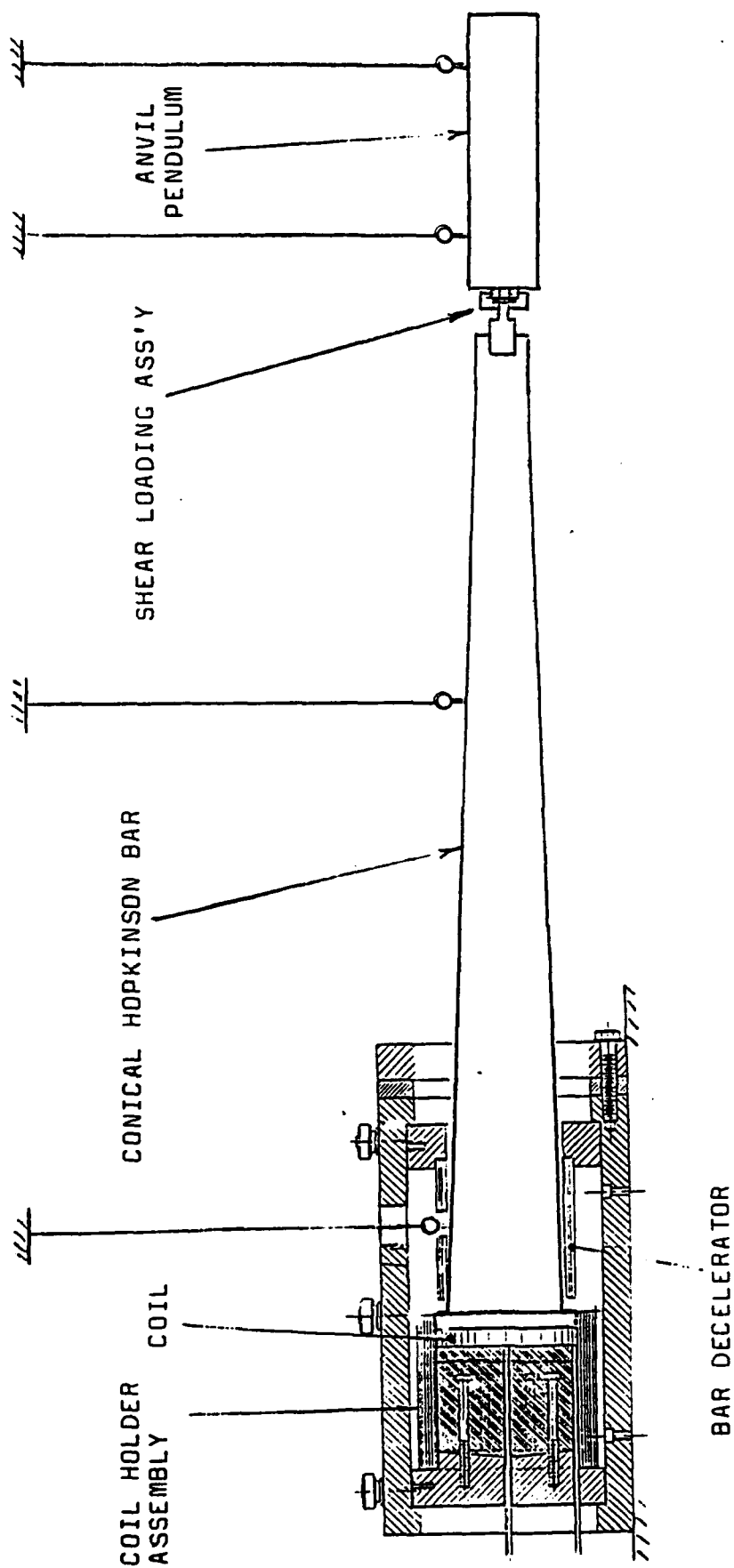$$Pt \quad N^2V^2C^{1\frac{1}{2}}L^{-\frac{1}{2}} \qquad\qquad (2)$$

- 6 -

FIG. 2   ELECTROMAGNETIC HOPKINSON BAR — SHEAR TEST CONFIGURATION
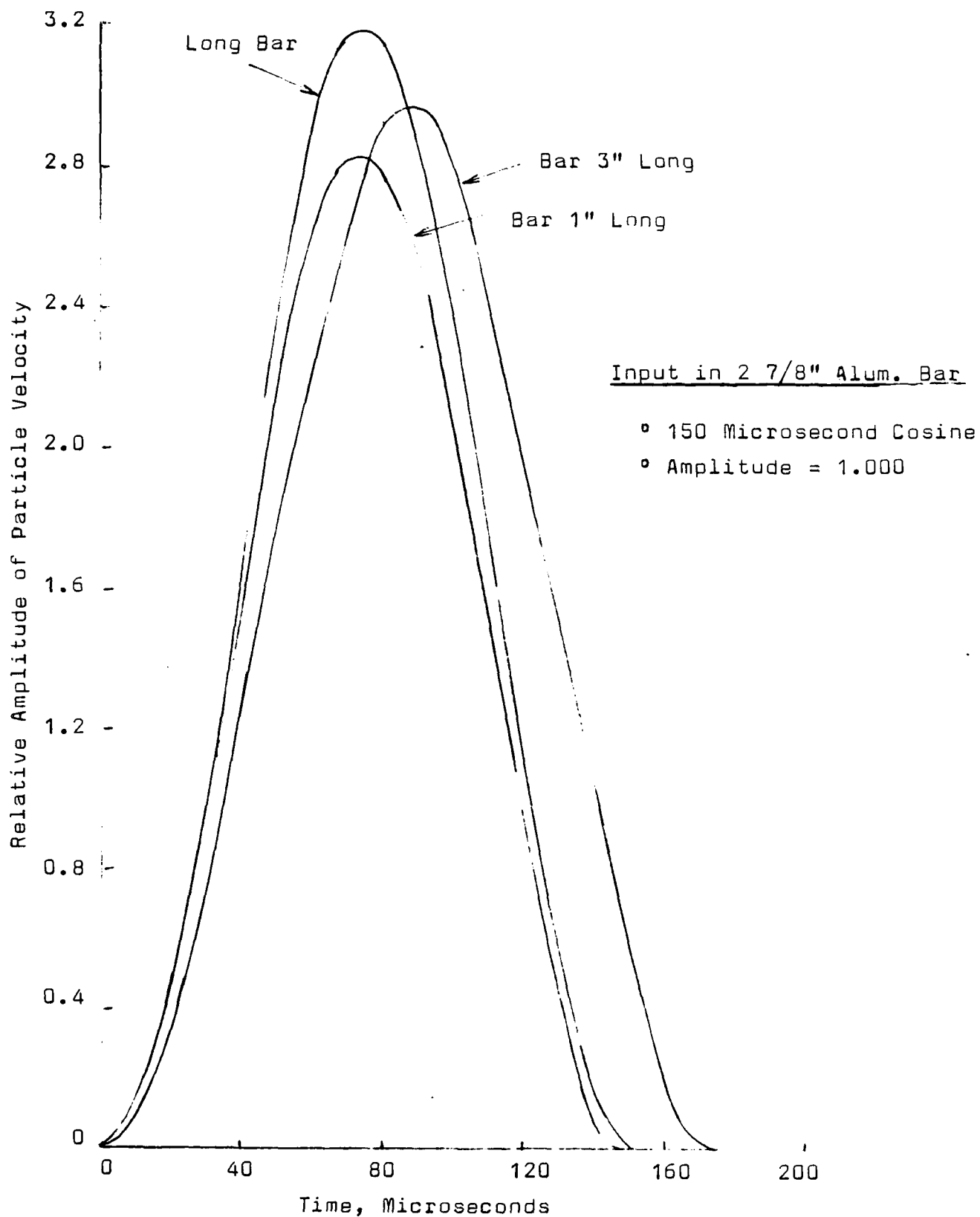
Fig. 3 Velocity vs. Time for 1½ Inch Steel Bar

Figure 4 is a plot of inductance of pancake coils versus number of turns, N. When re-plotted on log paper, the inductance of coils with N>10 is seen to be proportional to $N^{3.6}$. Combining this relationship with Equation 2 and with the pressure and load duration relationships:

$$Pt \sim N^{0.2}V^{2}C^{1.5} \tag{3}$$

$$P \sim N^{-1.6}V^{2}C \tag{4}$$

$$t \sim N^{1.8}C^{\frac{1}{2}} \tag{5}$$

Note that the current electromagnetic generator design consists of six (6) capacitors, the voltage can be varied from zero to 10 kilovolts, and the electromagnetic coil has eleven (11) turns. To maximize impulse (and, therefore, shear punch velocity) Equation 3 indicates little advantage in building coils with somewhat larger number of coils, since impulse varies with N to a small power. Using all six capacitors and running at the highest possible voltage is quite advantageous, however, for shear testing at the highest strain rates.

For obtaining stress-strain curves in tension, however, the strain rate is proportional to P/t:

$$\text{Tensile } d\epsilon/dt \sim N^{-3.4}V^{2}C^{\frac{1}{2}} \tag{6}$$

For maximum tensile strain rate tests, Equation 6 indicates the advantage of using the highest values of V and C, but it appears that coils with very small numbers of turns should be employed, based on rise time of the stress wave. Note, however, that the tensile specimen can be loaded by impact of a flat-ended bar similar to the shearing punch. This approach produces higher strain rates, which depend only on bar velocity and planarity of the impact.

Fig. 4 Coil Inductance vs. Number of Turns
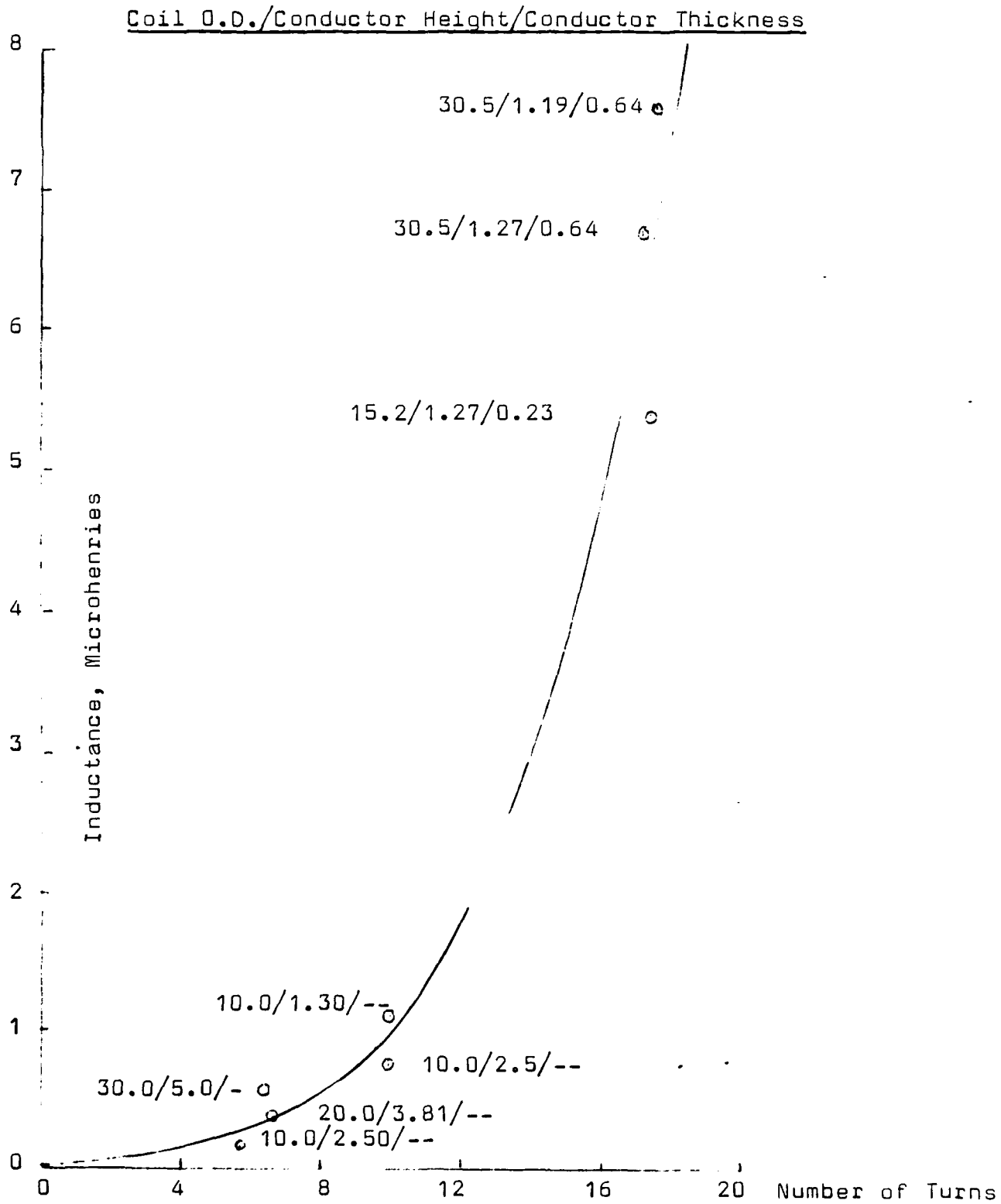
3.2 Hopkinson Bar Design & Performance

The purpose of the Hopkinson bar is to move the test samples and instrumentation away from the disruptive influences of the coil's intense electromagnetic field. In addition, the 34,200 psi stress input (at 10 KV input to the electromagnetic generator) to the eight-inch diameter end of the bar adjacent to the coil is amplified considerably by coning the bar down and focussing the stress waves toward the delivery end of the bar. In order to produce very high stresses, the following composite bar system may be employed:

(1) The aluminum bar is coned down from an eight inch diameter to a 2.875 inch diameter, where the stress amplitude is increased to 95,000 psi.

(2) Butted flat against the small diameter end of the bar is a 1.50 inch diameter steel bar, which experiences 300,000 psi when the stress wave crosses the aluminum-steel interface.

(3) Butted flat against the output end of the steel bar is a 0.75 inch diameter tungsten bar, which receives 790,000 psi when the stress wave crosses the steel-tungsten interface.

These stresses are only correct if each bar segment is long enough so that the peak stress in the input wave is developed before a reflected wave can reduce (or increase) the net stress at any particular station. However, the wave length of the input stress wave is approximately 30 inches in aluminum and steel and approximately 25 inches in tungsten (for the 150 microsecond duration associated with the coil in current use), and it is not desirable to make the steel and tungsten segments quite so long. Accordingly, it is necessary to make stress wave analyses of bar segments with a variety of lengths.

Figure 5 is a stress wave characteristic diagram for an aluminum cone 54 inches long, a steel bar 6 inches long, and a tungsten bar 10 1/8 inches long; corresponding to transit times of 270 microseconds, 30 microseconds, and 60 microseconds, respectively. These multiples of 30 microseconds were selected in order to minimize the proliferation of transmitted and reflected waves by insuring the maximum number of simultaneous arrivals of waves at each interface. However, this was done for computational convenience, and any segment lengths could have been selected for analysis.

The wave delivered to the large end of the cone (shown here as 6 1/2 inch diameter, since an 8-inch input end flange will be used to stop the aluminum cone's swing against a honeycomb crushup cylinder, resulting in a maximum input stress of 42,100 psi rather than the 34,200 psi input into the 8-inch diameter) is designated as an intensity of 1.000. This is multiplied by a factor of 2.261 in going from 6 1/2 inches to 2 7/8 inches, since stress is proportional to 1/R in a cone. Transmission and reflection factors are tabulated in the upper right hand corner of Figure 5, according to the equations for changes in area or impedance (see Ref. 5). At each interface, the intensity of an incident wave is increased or decreased in transmission and reflection by multiplying by these factors. For example, the 2.261 wave incident upon the aluminum-steel interface is multiplied by 3.158 to become the 7.140 transmitted wave, and by -.118 to become the -.267 reflected wave. At interfaces with air, the incident waves change sign and maintain the same amplitude.

Note that the segments remain in contact only when the net stress is compressive at the interface.. Figure 5 cannot indicate net stress at a station, since Figure 5 traces the history of a

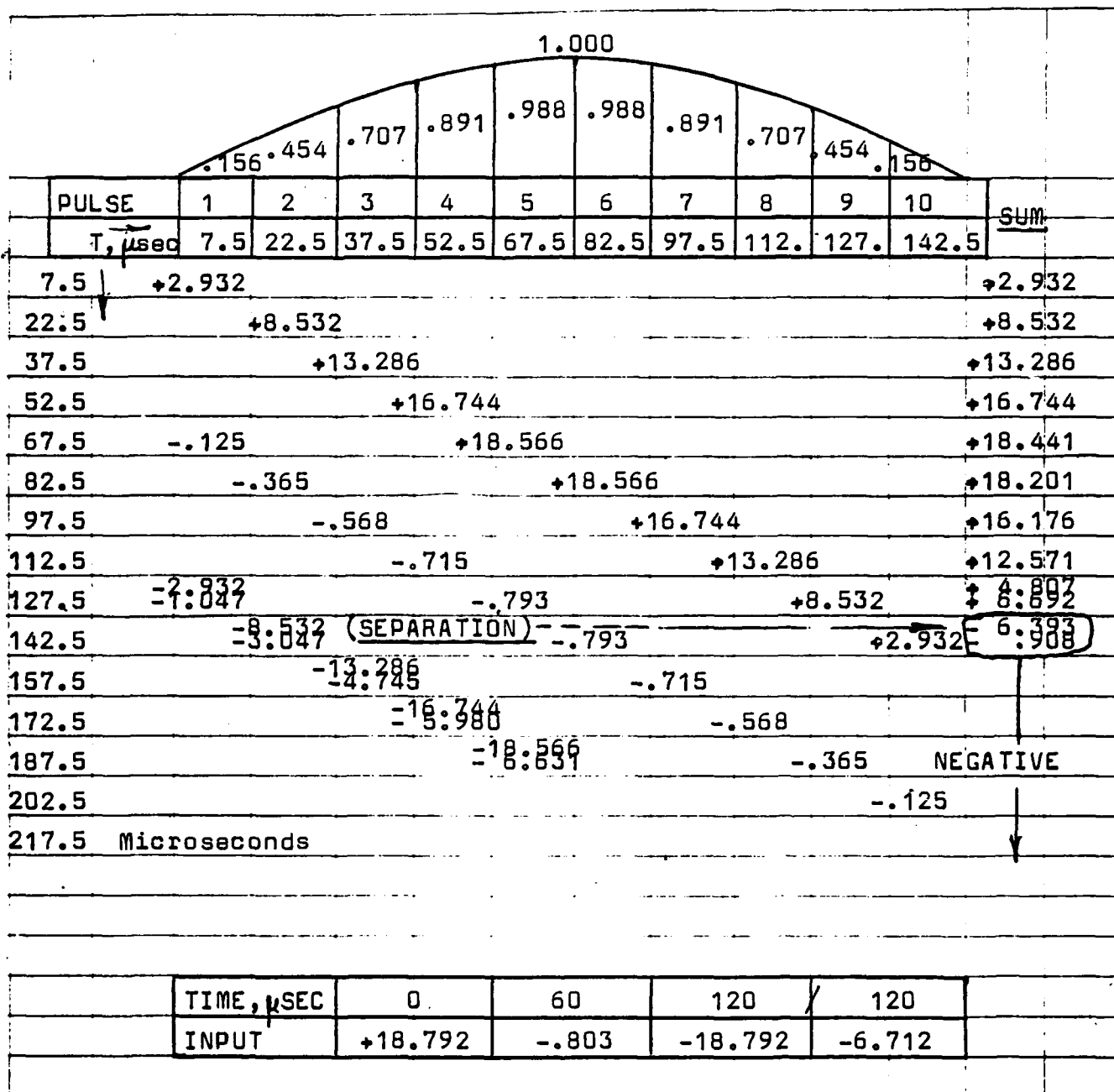# FIG. 5 STRESS WAVE CHARACTERISTIC DIAGRAM
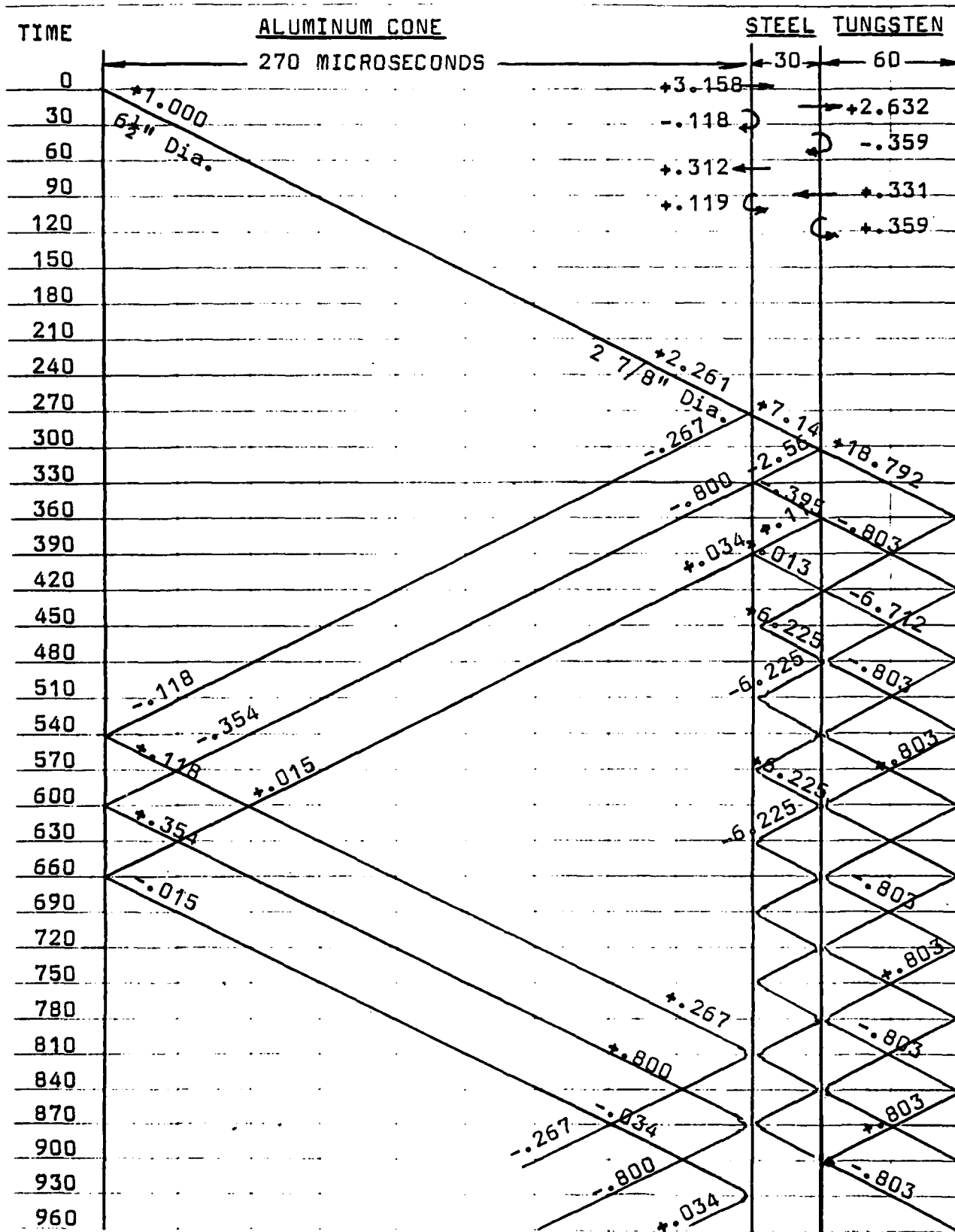
short duration pulse, and the net stress at any time will consist of the superposition of many pulses that were introduced to the origin at different times. A convenient bookkeeping system for keeping track of multiple pulses is illustrated by Figure 6.

In Figure 6 the input wave (shown here as a half-sine wave) is broken into 10 pulses, each 15 microseconds long. The mean amplitude of each pulse is shown under the sine curve, and the time of arrival of each pulse at the station in question in Figure 5 is also shown. At time 7.5 microseconds, for example, the pulse with amplitude .156 arrives at the station, followed in 15 microsecond intervals by pulses with amplitudes .454, .707, .891, .988, .988 ...... down to .156. Figure 6 pertains to the steel-tungsten interface. Figure 5 indicates that this interface first experiences a pulse with amplitude +18.792, based on an input of 1.000. Since the first input pulse had an amplitude of .156, the first arrival at the steel-tungsten interface has an amplitude of .156(18.792) = 2.932. Fifteen microseconds later the second pulse arrives, with amplitude .454(18.792) = 8.532. These numbers, all associated with the first sine wave with a maximum amplitude of +18.792, are followed by a second sine wave (60 microseconds later, as may be noted from Figure 5) with a maximum amplitude of -.803; then a wave of -18.792 at 120 microseconds, which changes immediately to -6.712. The table at the bottom of Figure 6 lists these wave arrivals.

The sums of the pulses arriving at the steel-tungsten interface are listed in the right hand column of Figure 6. At approximately 142.5 microseconds the net stress is negative, and the two segments separate. Accordingly, the next wave arrivals at that station will arrive at an air interface, as shown in Figure 5. A similar analysis of the aluminum-steel interface has been made,

- 14 -

FIG. 6   STRESS HISTORY AT THE STEEL/TUNGSTEN INTERFACE

PULSE	1	2	3	4	5	6	7	8	9	10	SUM
T, μsec	7.5	22.5	37.5	52.5	67.5	82.5	97.5	112.	127.	142.5	
7.5	+2.932										+2.932
22.5		+8.532									+8.532
37.5			+13.286								+13.286
52.5				+16.744							+16.744
67.5	-.125				+18.566						+18.441
82.5		-.365				+18.566					+18.201
97.5			-.568				+16.744				+16.176
112.5				-.715				+13.286			+12.571
127.5	-2.932 / -1.047				-.793				+8.532		4.802 / 8.892
142.5	-8.532 / -3.047	(SEPARATION)				-.793				+2.932	6.393 / 6.908
157.5	-13.286 / -4.745						-.715				
172.5	-16.744 / -5.980							-.568			
187.5	-18.566 / -6.637								-.365		NEGATIVE
202.5										-.125	
217.5	Microseconds										

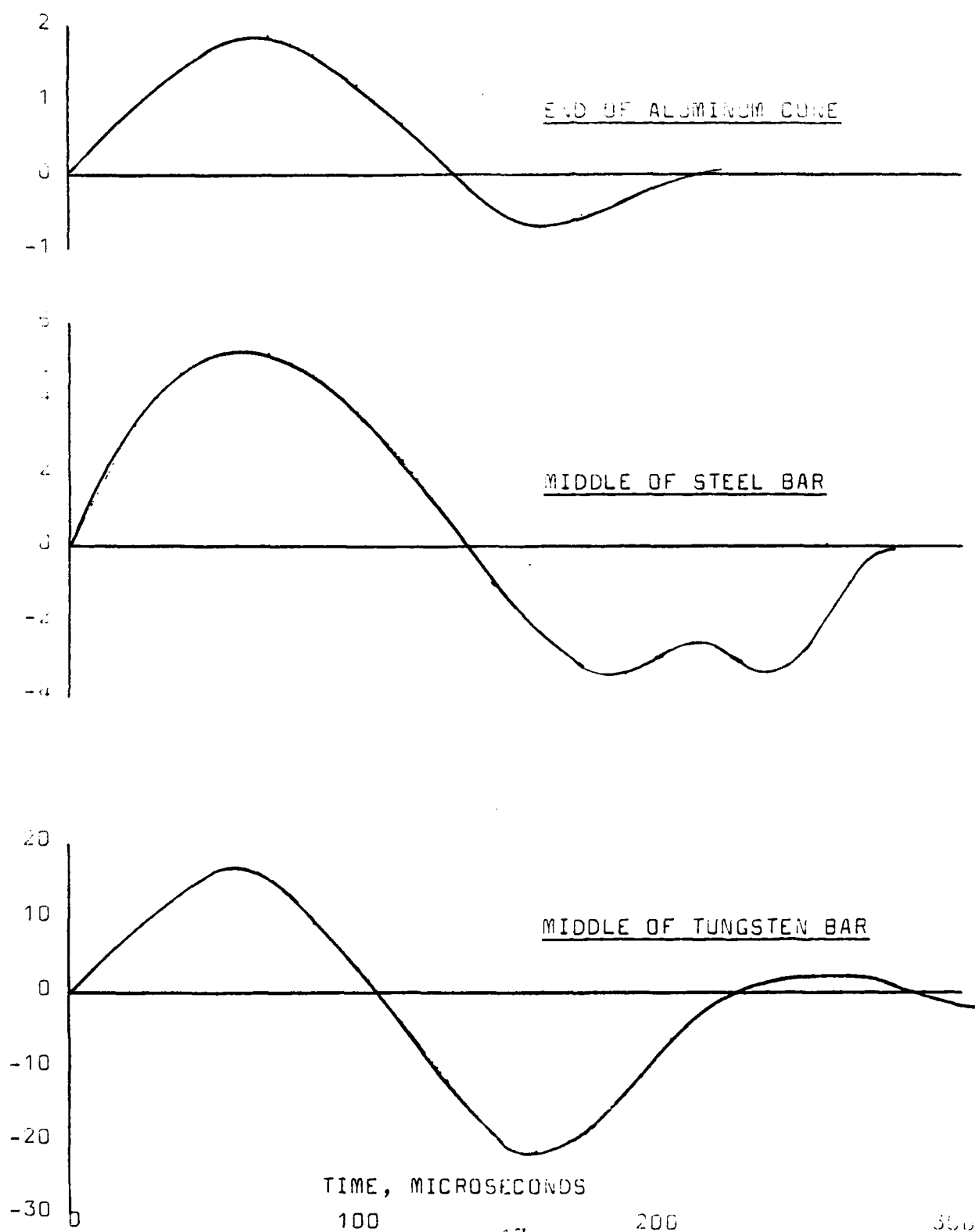| TIME, μSEC	0	60	120	120
INPUT	+18.792	-.803	-18.792	-6.712

- 15 -

and the results are also shown in Figure 5.

Diagrams similar to Figure 6 have been prepared in order to calculate stresses at the center of the tungsten bar, a the center of the steel bar and at various stations near the small diameter end of the aluminum cone. Figure 7 contains stress-time plots for an input intensity of 1.000. Peak stresses are presented in Table 1 for a 42,100 psi input (at 10 kilovolts).

STATION	MAX. COMP. STRESS, PSI	MAX. TENSION, PSI	PSI FOR LONG SEGMENTS
Near Small End of Alum. Cone	80,000	31,600	95,000
Middle of Steel Bar	219,000	147,000	300,000
Middle of Tungsten Bar	699,000	918,000	790,000

TABLE 1   PEAK STRESSES PRODUCED BY 150 MICROSECOND INPUT

For comparison, Table 1 also contains the stresses that would be produced in a Hopkinson bar system with long segments, and with no superposition of transmitted and reflected waves. Note that the actual stresses obtained at any section may be higher or lower than the nominal long-segment stresses, because of wave superposition and bar segment lengths. Wave analyses similar to those presented above may result in higher stresses delivered to the tungsten end of the EHB. However, the stresses shown in Table 1 are

- 16 -

FIG. 7 STRESS HISTORIES FOR 150 MICROSECOND UNIT INPUT

END OF ALUMINUM CONE

MIDDLE OF STEEL BAR

MIDDLE OF TUNGSTEN BAR

TIME, MICROSECONDS

- 17 -

considered high enough for conducting high strain rate tests on tungsten based composites.

Motion at the end of the Hopkinson bar may be calculated from the basic equation for particle velocity, u, in a stress wave, doubled to account for motion at the air interface:

$$2u = 2\sigma/\rho c \qquad (7)$$

The deflection that occurs because of a half sine wave with 150 microsecond duration will be equal to $0.636u(150\times10^{-6})$. For the 95,000 stress at the output end of the aluminum Hopkinson bar, with $\rho c = 0.100(203,000)$:

$$2u = 2(95,000)(386)/20,300 = 3,613 \text{ in/sec}$$
$$\delta = 0.636(3613)(150\times10^{-6}) = 0.345 \text{ inches}$$

For the steel punch, a calculation similar to the above using 300,000 psi in the steel results in a deflection of 0.385 inches. Note that stress and deflection will vary as applied voltage squared, according to Equation 4. Therefore, the motion of the end of the steel punch will only be $(0.2)^2(0.385) = 0.015$ inches for a 2 KV input and 0.035 inches for a 3 KV input. These are the gaps that should be left initially between the end of the punch and the test sample, in order for the punch to be launched with full velocity before it begins its punching action.

If 100 percent of the impulse at the 2.875 inch diameter end of the coned Hopkinson bar is transferred to the steel punch, the calculated value of velocity of the steel punch is 1,430 ft/sec. when the electromagnetic system is charged to 10 KV. The punch weighs 471.6 grams or 1.040 pounds. At 1,430 ft/sec its kinetic

- 18 -

energy is $\frac{1}{2}(1.040)(1430)^2/32.2$ = 33,000 ft-lbs. This is far greater than the energy required to shear through a 1/16 inch disk. A shear stress of 100,000 psi applied to a shear area of $\pi(0.5)(0.0625)$ results in a force of 9,820 lbs. Moving though a distance of 0.0625 inches, the shearing energy is 51.1 ft-lbs. The punch velocity is only 56 ft/sec to provide 51.1 ft-lbs of shearing energy.

Punch velocity is proportional to stress, which in turn is proportional to voltage squared. Table 2 contains calculated values of punch velocity and punch kinetic energy vs. input voltage.

Input KV	1	2	3	4	5	6	8	10
Punch Vel., ft/sec	14.3	57.2	129	229	358	515	915	1430
Punch KE, ft-lbs.	3.31	52.9	267	850	2070	4280	13500	33000

TABLE 2   KE OF PUNCH VS. INPUT KV

Table 2 indicates that the test disks with high shear strengths will not be punched entirely through at input voltages below about 2 KV. Some tests are conducted at low KV's, however, in order to be able to section the indented samples for evidence of shear banding. At the higher KV's, the punched-through test samples will provide shear band phenomenological data, as well as shear strength data at a range of strain rates.

Punch velocity may be measured indirectly by measuring pendulum swing, as discussed in Section 3.4. Figure 8 contains plots of punch velocity calculated on the basis that all the coil's impulse is transferred to the steel punch (curve labelled "theoretical"), as well as the punch velocity measured by impulse

Fig. 8 Punch Velocity vs. Kilovolt Input

Mass of Punch = 1.04 lbs.
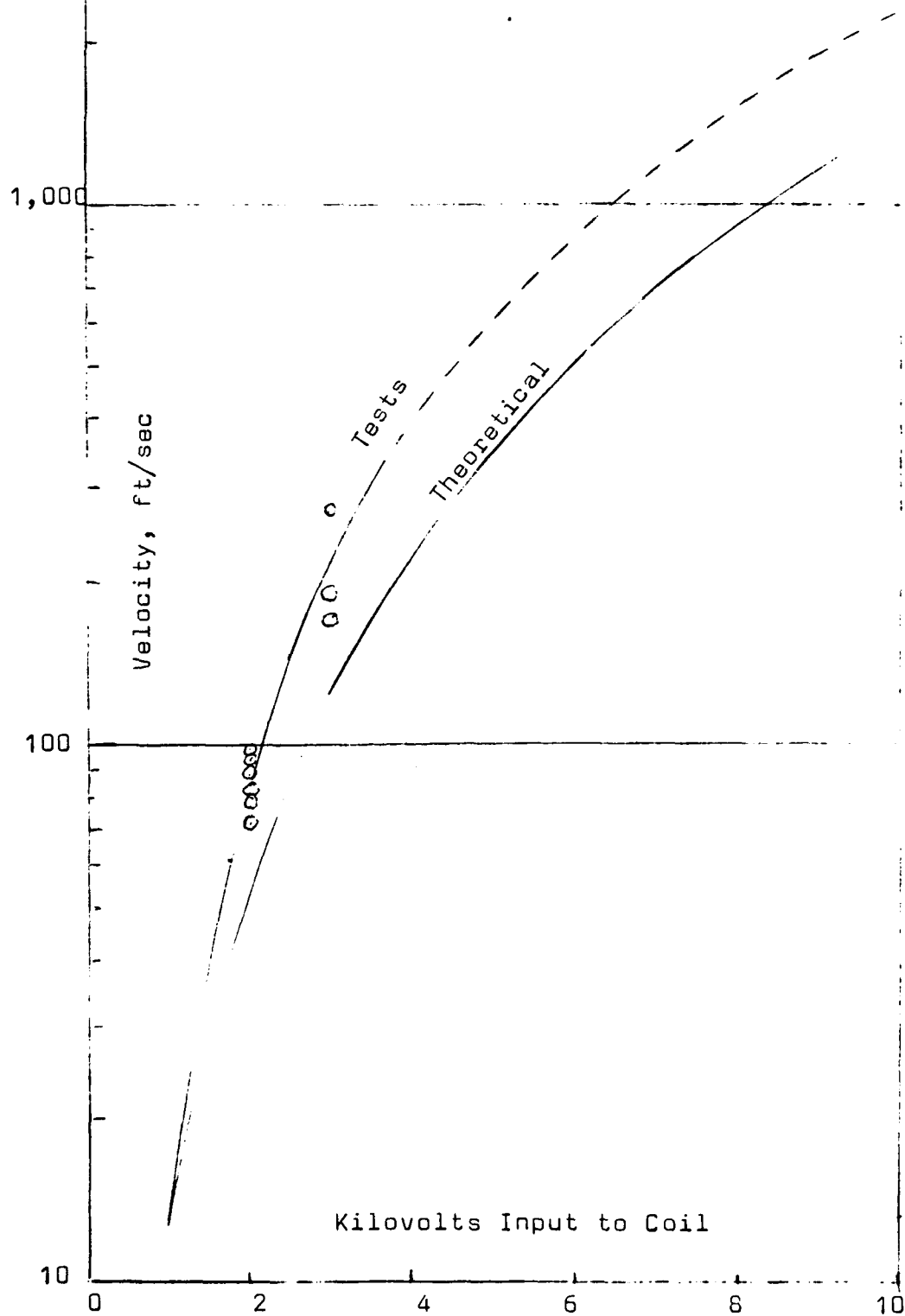
transfer to the pendulum. Note that the Hopkinson bar's output is higher than "theoretical". This apparent discrepancy is caused by the tension tail developed in the coned bar, which leads to motion of the bar back toward the coil and final bar velocity and momentum in the direction of the coil.

Strain rate in shear punch testing, calculated according to Equation 1 with the punch's diametral clearance of 0.0006 inches or radial clearance of 0.0003, is presented in Table 3 and plotted in Figure 9 vs. KV input. The velocity employed in these calculations was taken from the "tests" curve of Figure 8.

Input KV	1	2	3	6	10
Punch ft/sec	16	90	225	860	2200
Strain Rate, sec^{-1}	6.4×10^5	3.6×10^6	9.0×10^6	3.4×10^7	8.8×10^7

TABLE 3   STRAIN RATE IN DYNAMIC SHEAR TESTS

Table 3 indicates that punch velocities become somewhat excessive for operation of a laboratory facility and probably would require replacement of the punch and die system after each shot, for punch velocities above approximately 800 ft/sec. To prevent damage to the punch system, a punch "catcher" was installed (see Section 3.3) to transfer the punch's momentum to the massive coil mounting after approximately 3/8 inch punch travel. However, even the catcher system would probably be damaged when punch velocities are allowed to exceed approximately 1000 ft/sec. Accordingly, it is estimated that the practical limit of shear testing with this laboratory device will be of the order of 4×10^7 sec^{-1}. With throw-away test components, however, the upper limit of shear testing may be extended to approximately 10^8 sec^{-1}.

Fig. 9 Strain Rates with .0003" Punch Clearance
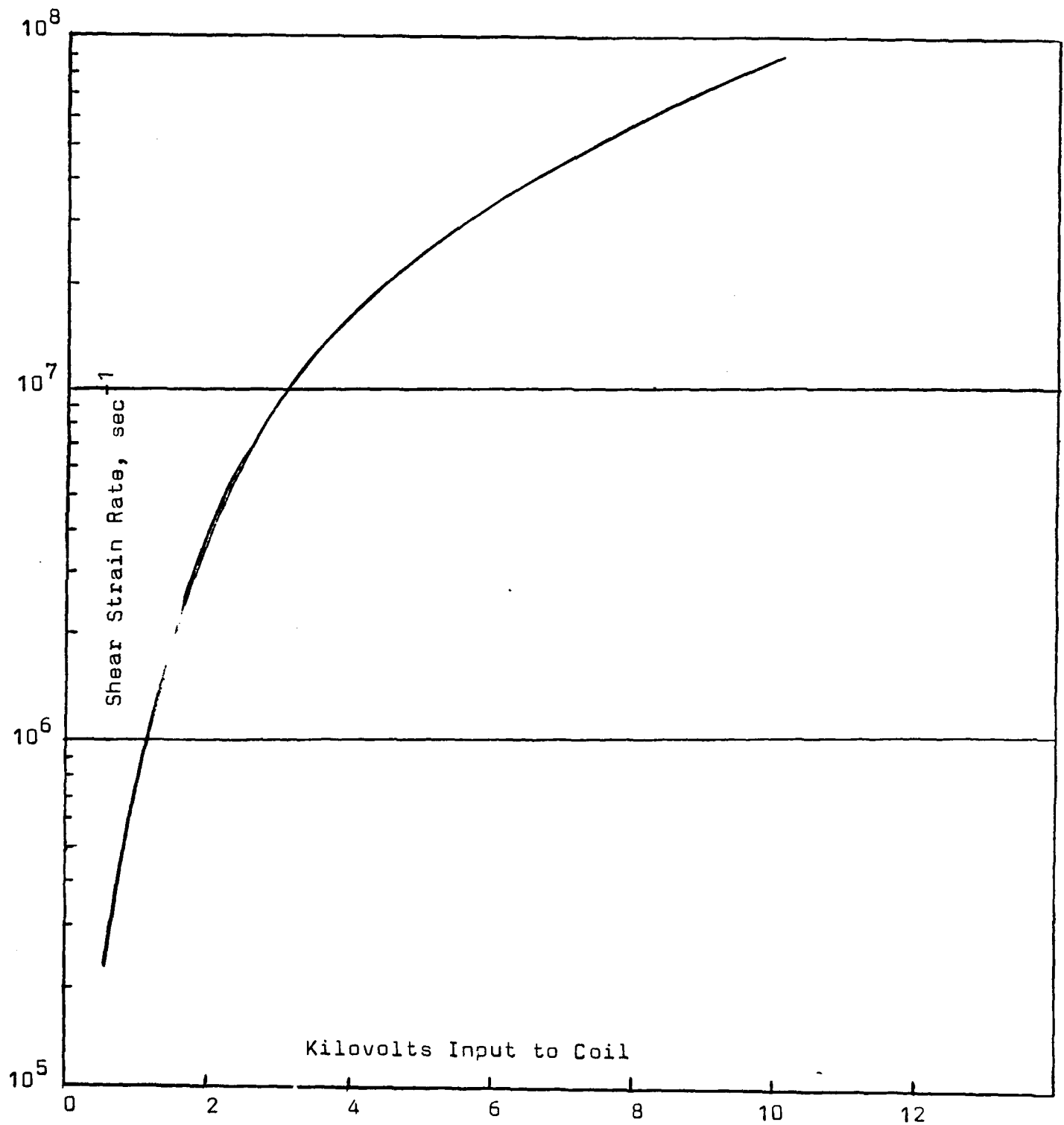
3.3 Shear Test Specimen & Fixture

The shear test specimens consisted of one-inch diameter disks with 0.0625 inch thickness. They were held in a steel punch-die assembly, as shown in Figure 10. For the overall facility configuration, refer to Figure 2. The punch catcher system serves two purposes:

(1) When the capacitors discharge into the electromagnetic coil and an impulse is delivered to the Hopkinson bar, the coil and its housing experience the same impulse and the entire housing moves to the left in Figure 2. This velocity to the left is cancelled by the punch momentum when the punch strikes the catcher, preventing excessive deflection of the coil's electrical system.

(2) The motion of the punch is stopped _after_ it shears through the test sample, and before it can impact against the die and force gage. If high velocity impact were allowed against the die and force gage, both would be damaged.

Two kinds of punch were evaluated, a flat-ended punch and a punch with its face ground to become a slant-ended punch with approximately an 8 degree slope. There are two advantages to be gained with the slanted punch. First, it allows a gradually increasing load to be delivered to the force gage, thus facilitating dynamic measurements. Second, it makes it possible to obtain a continuous range of strain rates developed in a single test specimen. The leading edge of the punch face shears through the test specimen at the highest velocity, while the trailing edge of the punch face shears through after the punch has been slowed down by the shearing resistance of the test sample. Measurements of dynamic force or punch deceleration will permit calculation of strain rate versus punch travel.

Figure 10. Shear Punch Assembly Drawing
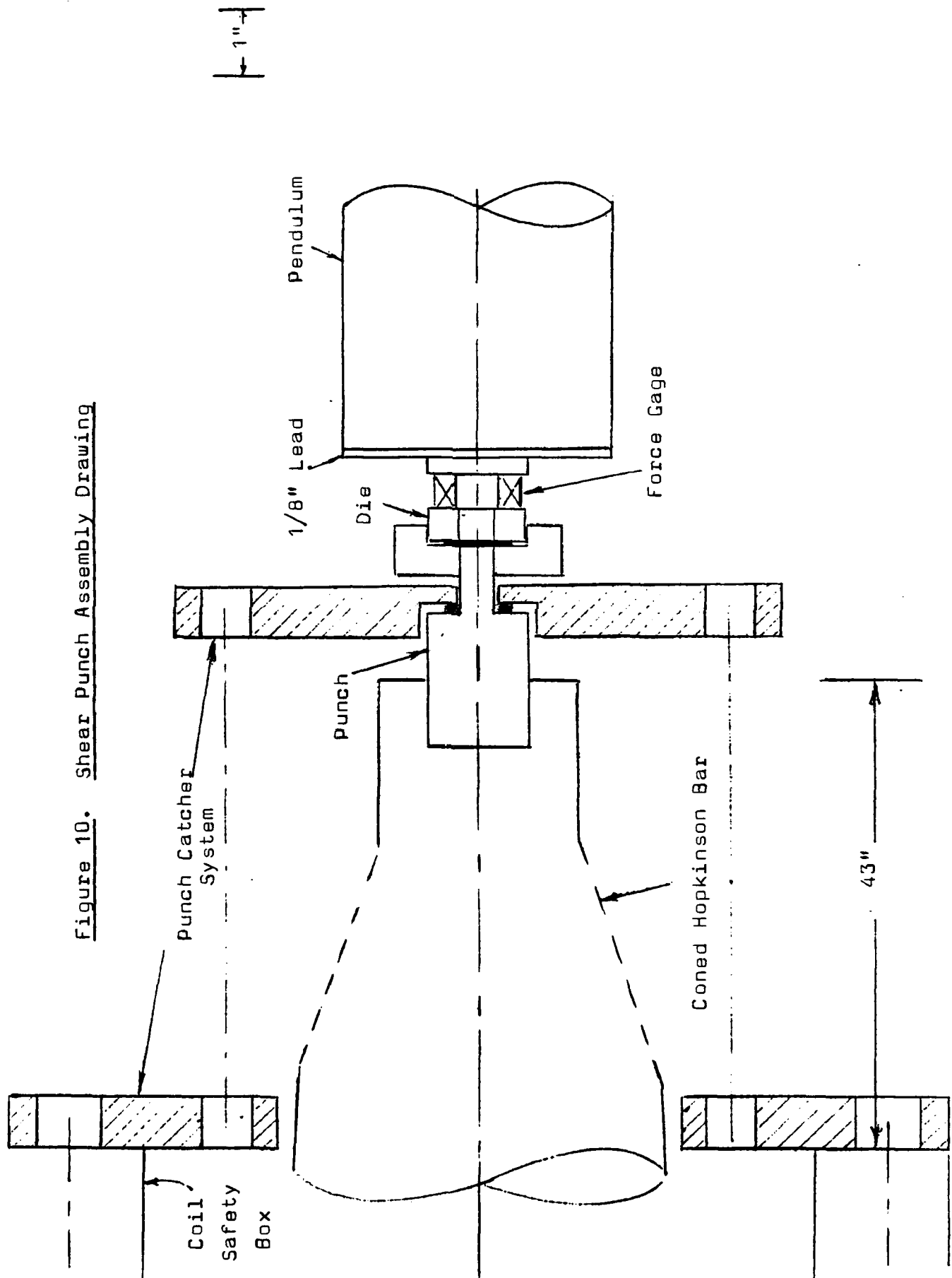
3.4   Instrumentation

It would be desirable to obtain some measure of shear resistance of the test sample. Of greatest value would be a force-time history of the shearing process and, secondarily, an indication of the impulse required to shear through the sample's thickness.   Figure 11, taken from Reference 6, shows how the impulse delivered to the test specimen can be expected to vary as velocity increases above the threshold value required for complete shearing out of the punched disk.

Normalized Impulse $I/M_0 V_{50n}$

$I/(M_0 V_{50n}) = V_0/V_{50n}$

$I/(M_0 V_{50n}) = V_0/V_{50n} - \sqrt{(V_0/V_{50n})^2 - 1}$

Data concerns 4.8-mm 7075-T6 aluminum alloy plate impacted by 0.25-g steel cubes ($V_{50n} = 850$ m/s)

Normalized Velocity V_0/V_{50n}
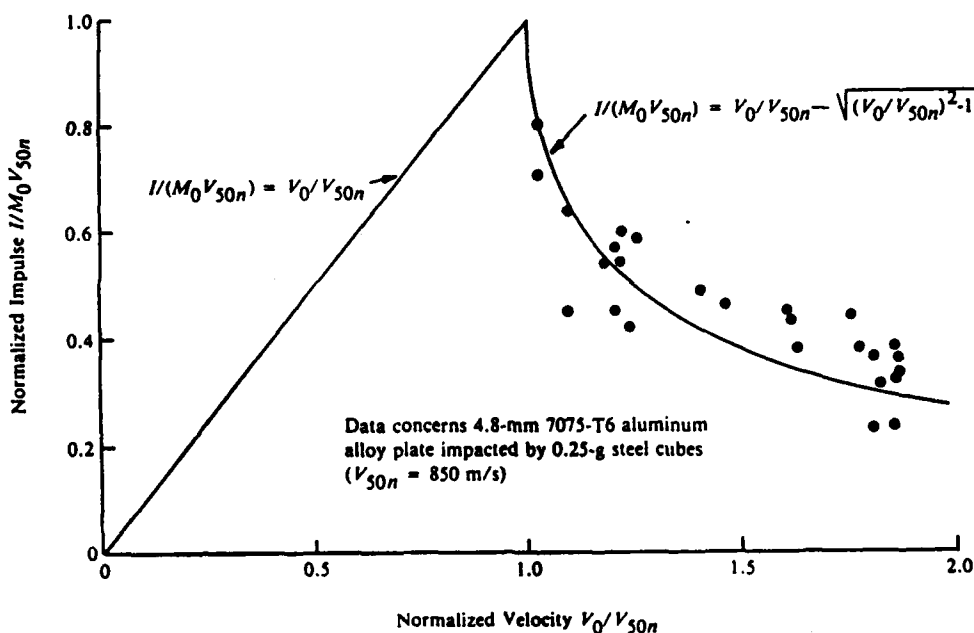
Fig. 11   Impulse Transmitted to Plate During Ballistic Perforation

The duration of loading on a sensor monitoring the shearing process is equal to disk thickness divided by punch velocity, for a flat-face punch.   At 3 KV, for example, Figure 8 indicates a

punch velocity of 225 ft/sec, leading to a loading duration of 23.1 microseconds for a flat punch of a .0625 inch thickness. If a dynamic sensor is required to record this pulse, its natural period should be less than approximately 1/4 the loading duration, or approximately 6 microseconds. This corresponds to a natural frequency of at least 167,000 Hz.

If the sensor is an accelerometer mounted on the rear end of the pendulum bar, as shown in Figure 12, the accelerations it experiences will be as shown (see Reference 7, p.68).

Experimental setup for study of stress waves.
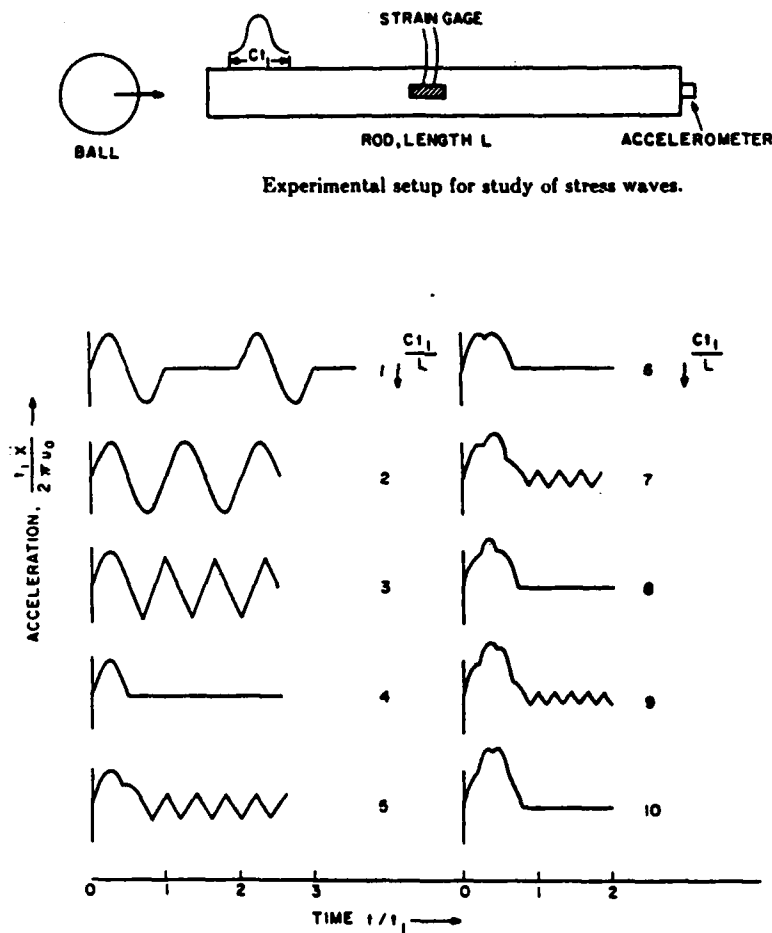
Fig. 12   Surface Accelerations Caused by Stress Waves in a Rod

With the pendulum bar length of 16.25 inches and Ct_1 = 30 inches, Ct_1/L = 1.846. Figure 12 indicates that an accelerometer will have an oscillatory response at period t_1, _if_ it is high enough frequency. If not, it will respond in its own natural frequency.

Figure 13 contains the response of an Endevco shock accelerometer Model 2225, claimed to have a mounted natural frequency of 110 kHz or a natural period of 9.1 microseconds. The oscillations recorded in Figure 13 have a period of approximately 66 microseconds. Note that Shot No. 25 was at 2 KV (or approximately 90 ft/sec) with a flat-face punch striking an aluminum disk and producing an indentation approximately .01 inches deep. The loading duration was of the order of 2(.01)/12(90) = 19 microseconds. It appears from this evidence that the natural period of the accelerometer was about 66 microseconds, which is too long to read the inputs accurately. To apply the accelerometer approach to measuring shearing forces, it appears that much higher frequency accelerometers must be employed.

A second method of measuring shearing force is to employ a dynamic force gage directly behind the punch, as shown in Figure 10. Many tests were conducted with a Kistler quartz force transducer, Model 9041, with a maximum force rating of 24,500 pounds and a natural frequency of 65 kHz. Note that this is the transducer's own natural frequency, without the mass of the steel punch added to the mass of its own structure. Figure 14 is the typical response of this force gage. The first positive swing of the gage has a duration of approximately 130 microseconds, regardless of test conditions. This would indicate that the gage is responding at its own (loaded) natural period of about 260 microseconds, which is _much_ too long to measure inputs of the order of 20 microseconds. It may be useful, however, as an impulse meter.

FIG. 13 OUTPUT OF ACCELEROMETER MOUNTED ON REAR OF PENDULUM, SHOT NO. 25

- 28 -
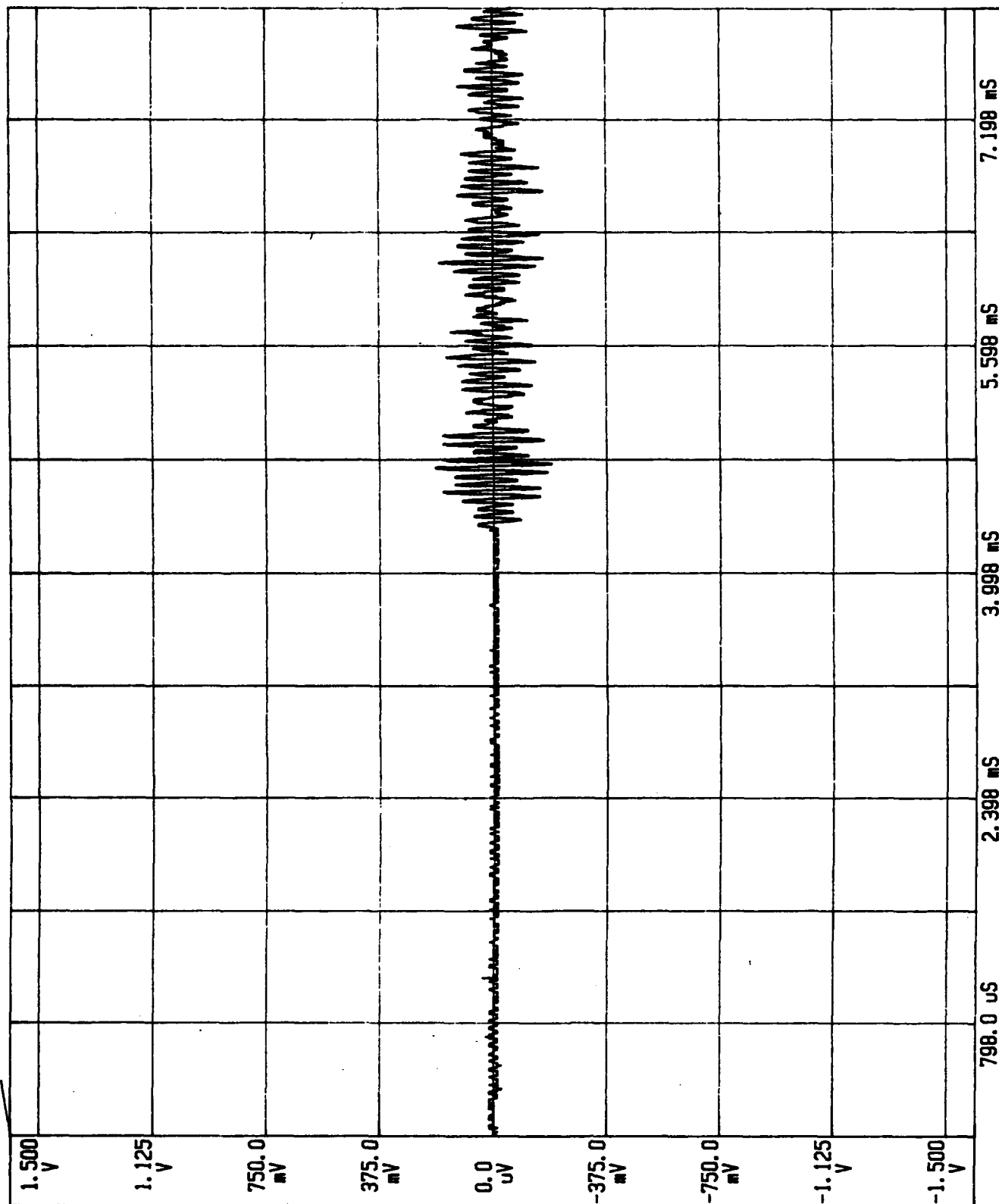
FIG. 14 OUTPUT OF A DYNAMIC FORCE GAGE, SHOT NO. 51
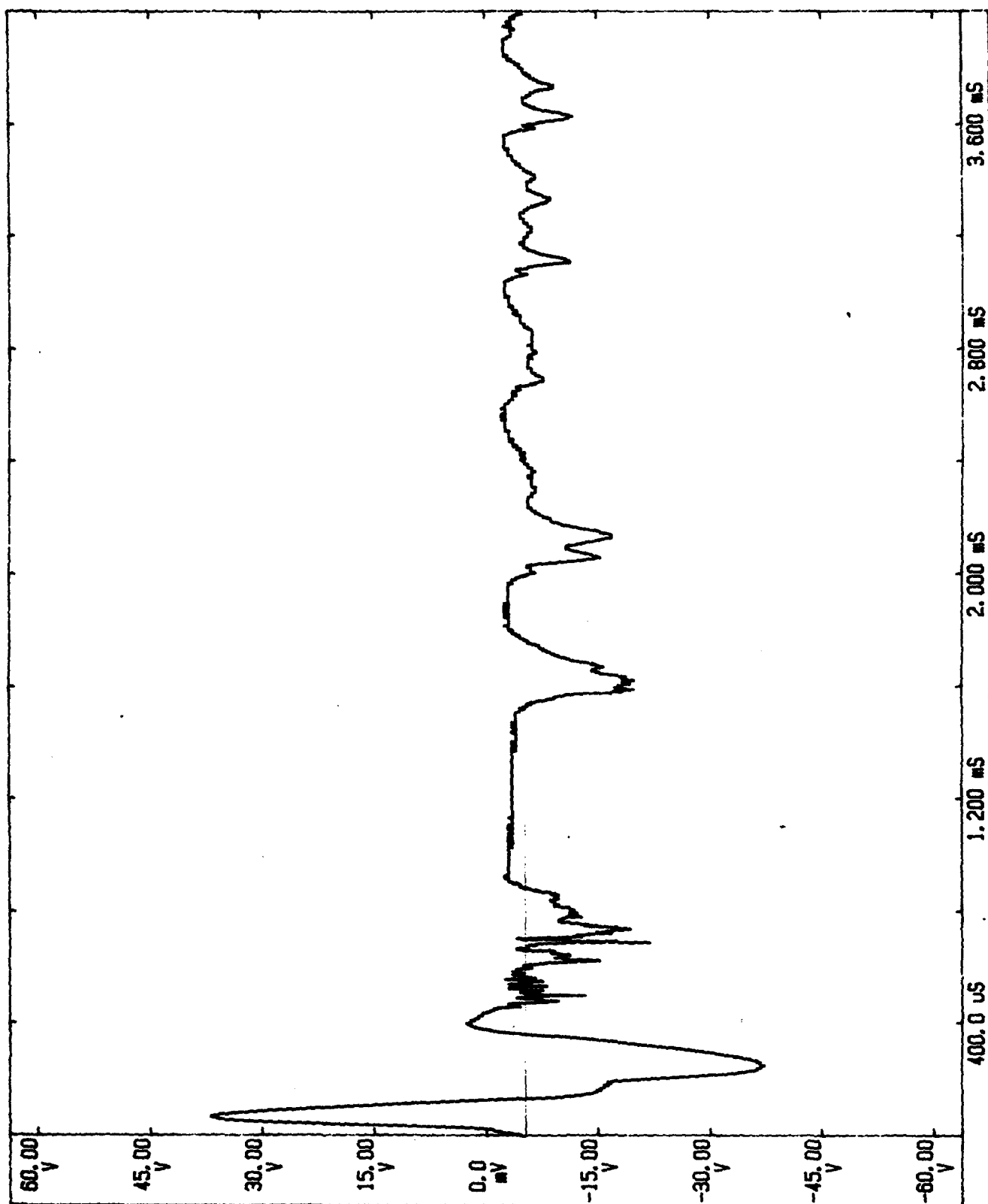
- 29 -

Figure 10 shows an 1/8 inch lead plate mounted directly behind the force gage, with a 1.38 inch diameter steel disk interposed between the two. This lead plate was intended to be a backup to the force gage, if the range of the force gage was exceeded. In addition, it could serve to measure impulse, as the indentation of the steel disk would provide a permanent record of force. In practice, however, the indentations were too shallow to be accurate indicators. Further, interpretation of the meaning of the lead indentations was expected to be controversial. Accordingly, this approach was abandoned in favor of using the pendulum as the primary impulse meter.

Punch velocity may be measured indirectly by measuring pendulum swing, as shown by Equation 8, where H is the height the pendulum attains in its swing, L is pendulum length (= 26") and X is the horizontal swing deflection:

$$X^2 = H(2L - H) \qquad (8)$$

Pendulum velocity v_p is related to H as follows:

$$v_p^2 = 2gH \qquad (9)$$

Punch velocity V is related to pendulum velocity according to the following no-bounce (if the punch strikes a soft lead plate mounted on the pendulum) momentum equation, where the pendulum weighs 57.8 lbs. and the punch weighs 1.040 lbs:

$$1.040 \ V = (1.040 + 57.8)v_p \qquad (10)$$

Calculations based on Equations 8, 9, 10 are presented in Table 4.

Input KV	2	3	4	5	6	8	10
Predicted V, ft/sec	57.2	129	229	358	515	915	1,430
v_p, ft/sec	1.01	2.28	4.05	6.33	9.10	16.2	25.3
H, inches	.191	.970	3.06	7.48	15.4	49.0	119
Swing X, inches	3.15	7.04	12.2	18.2	23.7	-	-

TABLE 4   PREDICTED PENDULUM SWING VS. KV INPUT

Preliminary tests have been conducted with the lead-faced pendulum, in order to measure punch velocity. The results are given in Table 5.

Shot No.	KV Input	Pendulum Swing, In.	Punch Velocity, Ft/Sec
30	1	.69	12.8
32	1	.84	15.5
14	2	5.30	98
15	2	4.30	79
16	2	4.03	73
17	2	4.97	91
18	2	5.13	94
19	2	5.00	91
31	2	4.56	83
33	2	5.12	93
20	3	14.0	275
21	3	10.2	192
34	3	9.1	172

TABLE 5   PUNCH VELOCITY OBTAINED FROM PENDULUM SWING DATA

The punch velocity data of Table 5 are plotted in Figure 8. Note that punch velocity tests were not conducted at higher KV inputs. The electromagnetic coil was exhibiting distress in the

form of arcing across its insulation, and it was decided to reserve the possibly damaging high-KV shots for tests of tungsten composite samples. However, in preparation for the time when the coil could be repaired or replaced, a 200 pound pendulum was fabricated. This pendulum could obtain punch velocity data without an excessive amount of horizontal swing, as shown in Figure 15.

The combination of instrumentation sensors recommended for further shear testing is the pendulum for measuring initial velocity of the punch as its starts its shearing action, and a high frequency accelerometer mounted on the pendulum to measure shearing resistance versus time. Note that the accelerometer's frequency requirements may be relaxed from the 167 kHz estimate made above. This may be accomplished by two means:

(1) By using a slant-face punch, loading duration t_1 may be increased. If, for example the punch face slant is at 45 degrees and its diameter (or length, if it is a rectangular punch face) is 0.75 inches, and it impacts the test sample at 225 ft/sec as previously assumed, the load duration is
(0.0625 + 0.75 tan 45)/225x12 = 300.9 microseconds. This is 13.0 times the 23.1 microseconds calculated for flat-face impact, which translates to an accelerometer frequency requirement of 167/13.0 = 12.8 kHz. Endevco's shock accelerometers should do it easily.

(2) The 200 pound pendulum length is 11.0 inches. The parameter Ct_1/L corresponding to the 300.9 microsecond durations associated with the 45 degree slant punch = (0.20)(300.9)/11.0 = 5.47. Entering Figure 12 at Ct_1/L = 5.47, it appears that this will be in a regime ($Ct_1/L > 4$) where the shearing pulse is distinctly different from the post-pulse ringing.

The above approach should permit good measurements of shear force versus time.

- 32 -

Fig. 15   Horizontal Swing of Pendulum

Impact Mass = 1.04 Lbs.

Length = 26 Inches
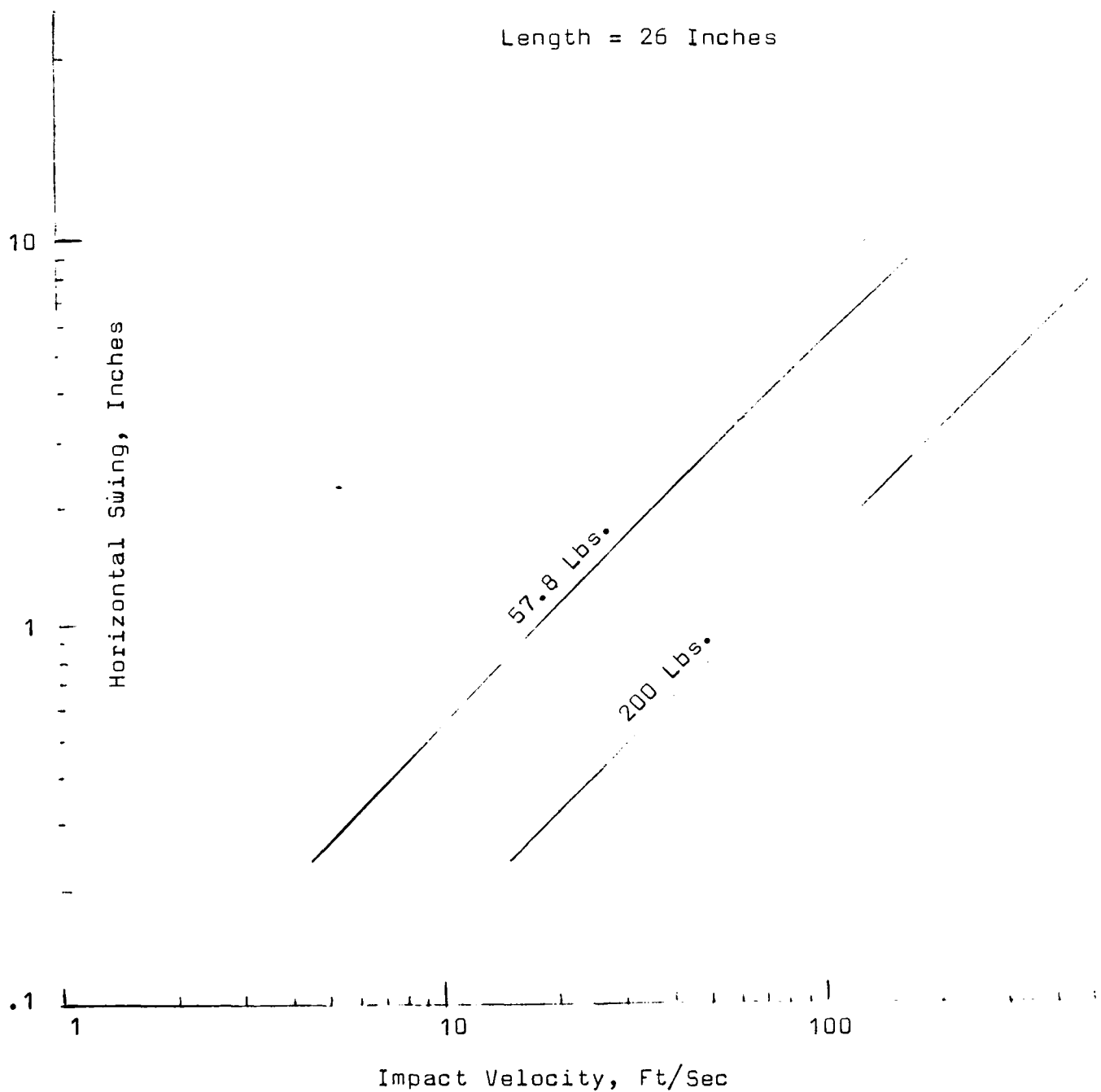
Note that it is theoretically possible to obtain force versus time from impact velocity and impulse measurements. However, two assumptions would be required. First, the shape of the force-deflection curve would have to be assumed. Second, it would be necessary that only the shearing impulse is measured. This latter condition does not exist with the punch system as it presently exists, since it is found that the sheared disks tend to jam in the die and continue to provide resistance after the shearing action is over. Although the die could be designed to minimize this effect, the accelerometer approach is recommended for future development.

4. TEST RESULTS

4.1 Test Data

Table 6 contains the test data for tests with the tungsten composite samples, consisting of disks 0.0625 inches thick and 1 inch diameter. Punch velocities are taken from Figure 8 rather than from pendulum swing measurements, since these latter measurements include impulse delivered only until the punch reaches the punch catcher system. Strain rates are taken from Figure 9, corresponding to the punch velocities.

SHOT	SAMPLE	TEMP. Deg. F	PUNCH FACE	PUNCH V, FT/SEC	STRAIN RATE X 10^{-6} SEC^{-1}	PUNCH THRU	SHATTER
35	Coated	Room	Slant	90	3.6	–	–
36	95% W	"	Flat	"	"	–	–
59	"	530	"	"	"	–	–
47	"	Room	Slant	225	9.0	X	X
51	"	"	Flat	"	"	X	X
60	"	520	"	"	"	X	X
62	"	550	Slant	"	"	X	–
37	Zr Foil	Room	Flat	90	3.6	–	–
40	"	"	Slant	"	"	X	X
50	"	"	Flat	225	9.0	X	X
56	"	420	"	"	"	X	X
57	"	420	"	"	"	X	X
63	"	550	Slant	"	"	X	X
41	30% Ti	Room	"	90	3.6	X	X
44	"	"	Flat	"	"	X	X
61	"	540	"	"	"	X	X
65	",Anneal.	Room	Slant	"	"	X	X
68	" "	470	"	"	"	X	X
42	40% Ti	Room	"	"	"	X	X
45	"	"	Flat	"	"	X	X
53	"	280	Slant	"	"	X	X
54	"	470	"	"	"	X	X
66	" Anneal.	Room	"	"	"	X	X
69	" "	570	"	"	"	X	X
43	50% Ti	Room	"	"	"	X	X
46	"	"	Flat	"	"	X	X
55	"	590	Slant	"	"	–	–
58	"	530	Flat	"	"	X	X
64	"	540	Slant	225	9.0	X	X
67	" Anneal.	Room	"	90	3.6	X	X
70	" "	560	"	"	"	X	X
38	GTE	Room	Flat	"	"	–	–
39	"	"	Slant	"	"	–	–
48	"	"	"	225	9.0	–	–
49	"	"	"	"	"	–	–
52	"	"	Flat	"	"	–	–
71	"	500	Slant	"	"	X	–
72	"	Room	"	400	15.7	X	–
73	"	"	"	605	23.7	X	–
74	"	"	Flat	"	"	–	–

TABLE 6   TUNGSTEN COMPOSITES TEST DATA

4.2 Dynamic Shear Behavior of Test Samples

Photographs were made of the test samples after dynamic testing in the punch-die assembly, and before sectioning and examination for evidence of adiabatic shear banding - see Figures 16 through 18. These figures provide more detail on the degree of fragmentation of each test sample, above and beyond the listing in Table 6 as either shattered or not by the punching process.

Table 6 indicates that most of the HIPed samples shattered during the punching process, if the sample was sheared entirely (denoted "punch thru" in Table 6) out of the original test disk. Indeed, one sample of 30% Ti by volume was brittle enough to be shattered while tapping the die closed with a hammer. Only one HIPed sample was punched through without shattering; Sample No. 62, which consisted of 95.4% W, 3.0% Ni, 1.6% Fe which had been pre-heated to 550 degrees F. It may well be that these HIPed materials will all become more ductile if heated sufficiently. However, in view of the fact that shock-induced temperatures will probably remain below the pre-heat temperatures employed, it appears that other means of introducing ductility will be required with HIPed tungsten composite materials.

Some measure of shearing strength may be obtained by determining the threshold punch velocity for complete punching of the test sample. Although this approach of determining V_{50} as in Figure 11 was not attempted in Phase I because of the small number of the test samples, Table 6 does contain some usable data of this kind. See Table 7.

Relative resistance to shear may be deduced from Table 7. The GTE liquid phase sintered material is strongest, the 95% W HIPed material is next, while all the other materials were punched through at the lowest velocity.

FIG. 16   POST-TEST APPEARANCE OF TEST SAMPLES

TOP = 95% W
BOTTOM = Zr FOIL
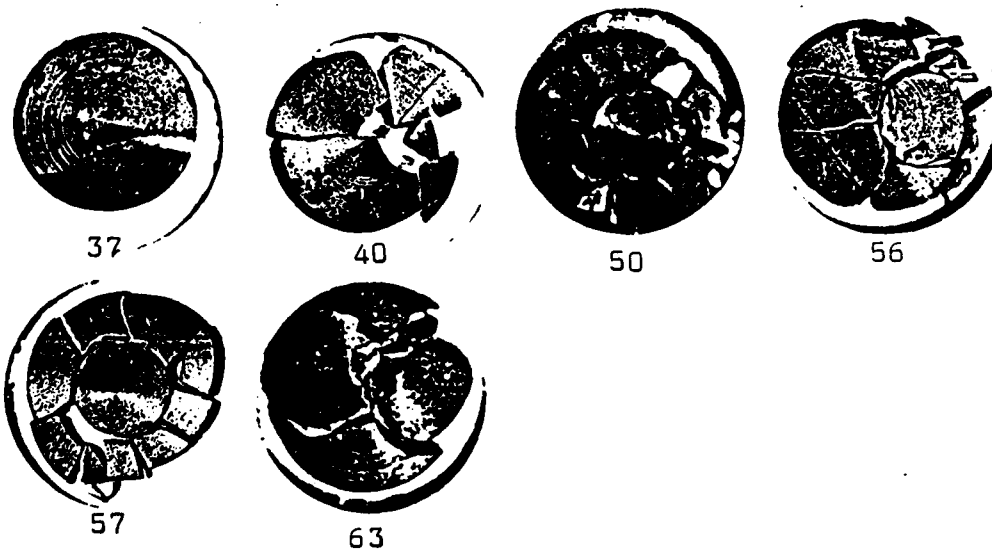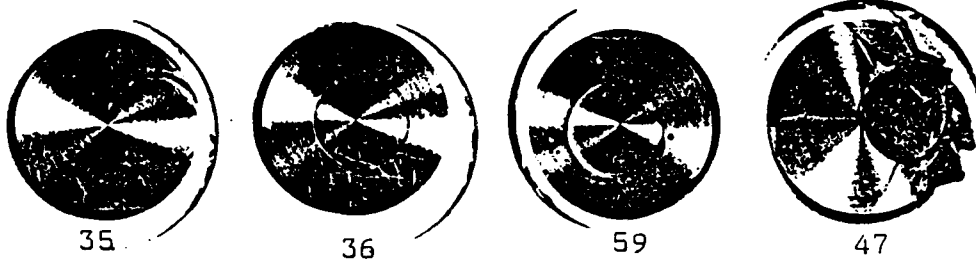
FIG. 17   POST-TEST APPEARANCE OF TEST SAMPLES

TOP = 30% Ti, MIDDLE = 40% Ti, BOTTOM = 50% Ti
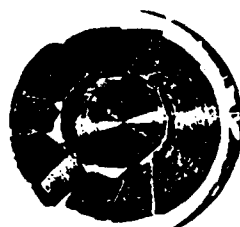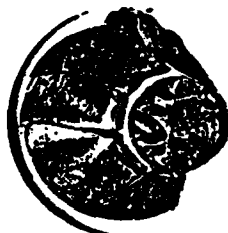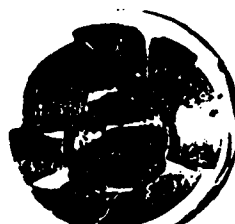
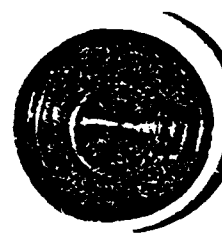FIG. 18   POST-TEST APPEARANCE OF GTE TEST SAMPLES
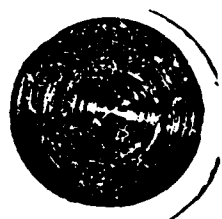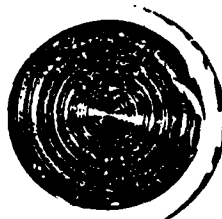
38   39   48
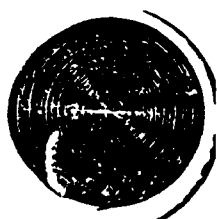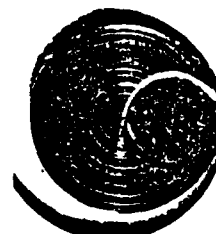
49   52   71
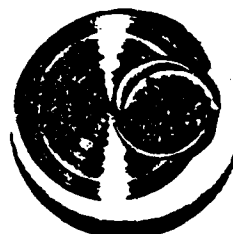
72   73   74

MATERIAL	PUNCH FACE	DID IT PUNCH THROUGH (AT V, FT/SEC) ?				
		V=90	225	400	605	Est. Threshold
95% W	Flat	No	Yes	-	-	158 ft/sec
	Slant	No	Yes	-	-	158
Zr Foil	Flat	No	Yes	-	-	158
	Slant	Yes	Yes	-	-	<90
30% Ti	Flat	Yes	-	-	-	<90
	Slant	Yes	-	-	-	<90
40% Ti	Flat	Yes	-	-	-	<90
	Slant	Yes	-	-	-	<90
50% Ti	Flat	Yes	-	-	-	<90
	Slant	Yes	-	-	-	<90
GTE-LPS	Flat	No	No	-	No	>605
	Slant	No	No	Yes	Yes	313

TABLE 7   VELOCITY FOR PUNCHING THROUGH AT AMBIENT TEMPERATURE

A highly approximate estimate of the threshold velocity required for complete punching of the test sample is the average of the highest no-punch velocity and the lowest velocity that produced complete punching. These approximate velocity thresholds are given in Table 7. Table 8 contains these threshold estimates, presented in terms of the kinetic energy of the 1.04 pound punch at the threshold velocity for complete punching.

MATERIAL	FLAT	SLANT
(GTE) LPS 90%W	>5,910	1,580
CWP 95%W	403	403
Zr-W Lam.	403	<130
W-Ti	<130	<130

TABLE 8   THRESHOLD KINETIC ENERGY FOR COMPLETE PUNCHING, FT-LBS

4.3 Metallographic Examination of Tested Samples

Due to the large number of samples tested, not all of them could be examined in the limited time available. Samples were selected with particular attention to establishing a proper baseline, and those that displayed behavior thought to be associated with adiabatic shear localization. The choice of samples also lends itself to comparisons of materials and test conditions. For example, it will be possible to compare the effects of a flat punch against the slant punch, room temperature versus elevated temperature and most importantly, one material versus another. Table 9 redisplays the relevant information from Table 6 for those samples examined metallographically.

TABLE 9. SAMPLES SUBJECTED TO METALLOGRAPHIC EXAMINATION

Sample Number	Short Description	Input KV	Test Temperature	Punch Type
39	LPS 90%W	2	Ambient	Slant
49	LPS 90%W	3	Ambient	Slant
72	LPS 90%W	4	Ambient	Slant
73	LPS 90%W	5	Ambient	Slant
71	LPS 90%W	3	500°F (260°C)	Slant
52	LPS 90%W	3	Ambient	Flat
59	CWP 95%W	2	530°F (275°C)	Flat
62	CWP 95%W	3	550°F (290°C)	Slant
35	CWP 95%W	2	Ambient	Slant
50	Zr-W Lam.	3	Ambient	Flat
55	W-50% Ti	2	590°F (310°C)	Slant
53	W-40% Ti	2	280°F (140°C)	Slant
44	W-30% Ti	2	Ambient	Flat

Note: LPS = liquid phase sintered, CWP = coated tungsten powder

The liquid phase sintered material is a 90% tungsten heavy alloy supplied by GTE Products Corporation of Towanda. PA. This material is used as a baseline because its properties and performance are well known (Reference 8). All other materials

tested were hot isostatically pressed (HIPed) by Industrial Materials Technology (IMT) of Andover, MA. A description of the HIP conditions used by IMT, for each material combination, is given in Appendix A. The coated tungsten powder was developed and produced by Ultramet, Inc. of Pacoima, CA (References 9, 10, 11).

4.3.1 Liquid Phase Sintered Tungsten Heavy Alloy

The GTE liquid phase sintered tungsten heavy alloy was chosen as the baseline material. Its composition was 90% tungsten, 8% nickel and 2% iron. The 8:2 nickel to iron ratio has recently been shown superior to the more traditional 7:3 ratio (Reference 8). The samples tested at room temperature with the slant face punch were examined first following a comparison to elevated temperature and flat face punch testing.

Sample 39 did not punch through and no evidence of shear localization was observed in the region of the punch strike. The bulk microstructure is shown in Figure 19 and the microstructure in the region of the strike is shown in Figure 20. In these figures the tungsten grains are the round particles and the matrix in the phase surrounds them. The microstructure for this sample and all of the GTE supplied samples (except as noted) appeared normal for heavy alloys.

Sample 49 was at first thought to have not punched through. Examination of the metallographic sample shows that there was complete failure at the periphery of the struck region but the slug did not release. Figure 21 shows the region of failure, and is typical of the cross section. It is of great interest to observe that, in the area of failure, where the shear strain was less than required for failure, the tungsten-to-tungsten grain contacts were failing earlier than the alloy matrix. This observation has
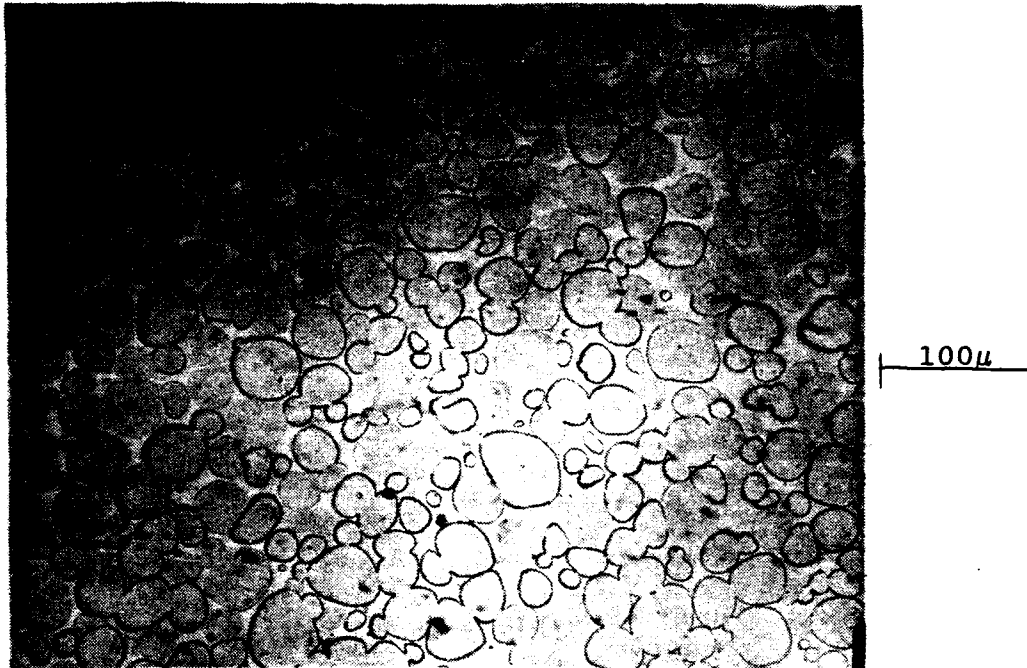
Figure 19.   Bulk Microstructure of #39, LPS 90%W, 200x
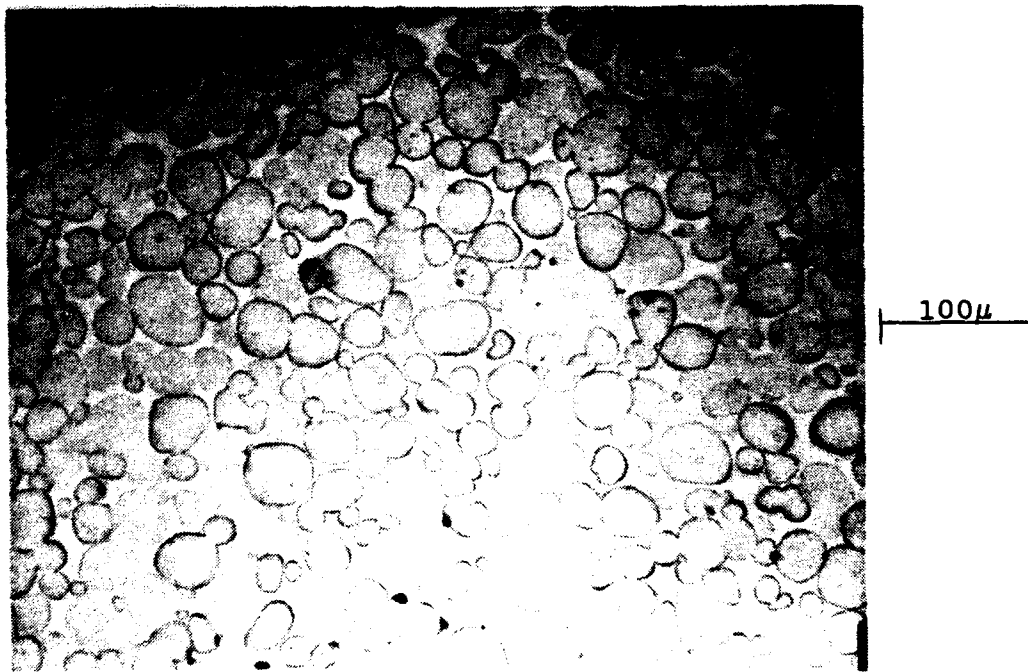
Figure 20.   Region of the Strike, #39, 200x

previously been made for similar alloys when tested at quasi-static and elevated strain rates (References 12, 13, 14, 15, 16). This is a clear indication that these contacts are the weak links in the heavy alloy microstructure and this weakness is present at elevated strain rates.

Sample 72 shows greater deformation of the tungsten grains in the region of maximum shear, Figure 22. This extreme deformation of the tungsten grains was not unexpected, but there is a lack of the previously observed tungsten grain contact failures. Extreme ductility of tungsten is not the norm in pure tungsten as it is usually characterized by a high degree of brittleness. But, in tungsten heavy alloys, the tungsten grains are capable of undergoing great amounts of deformation due to the ability of the matrix to apply a hydrostatic stress component that postpones failure to much greater strains (Reference 17). This extreme deformation of the tungsten grains has been observed, for example, in the examination of ballistically tested fragments, Figure 23 (References 18, 19).

Sample 73 is like sample 72, but showing much greater amounts of deformation of the tungsten grains in the region of maximum strain, Figure 24.

Sample 71 was tested under the same loading conditions as sample 49, except it was tested at 500°F (260°C). Sample 71 exhibited much greater ductility than sample 49; this is seen in Figure 25. This figure shows the region of the punch strike and the lack of general failure. What is seen is the tungsten-to-tungsten grain contact failure and a much greater grain size than the room temperature samples. It is possible, due to the method of heating, that greater than 500°F was seen by the sample, and grain growth resulted. It is also possible that this sample is of a
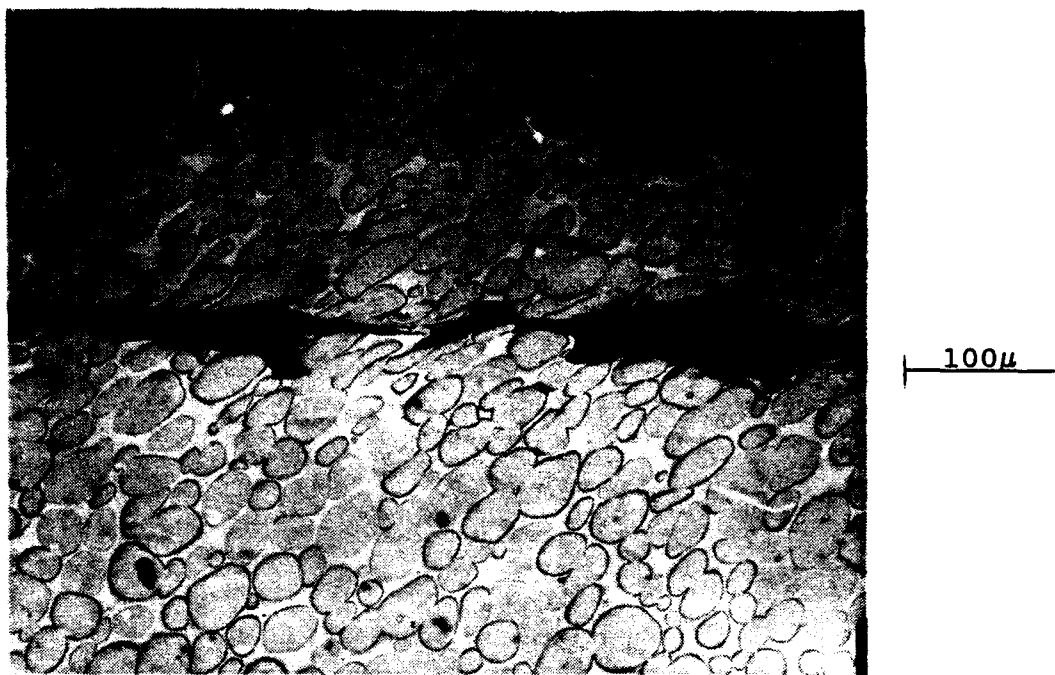
Figure 21.   Region of Failure, #49, LPS 90%W, 200x
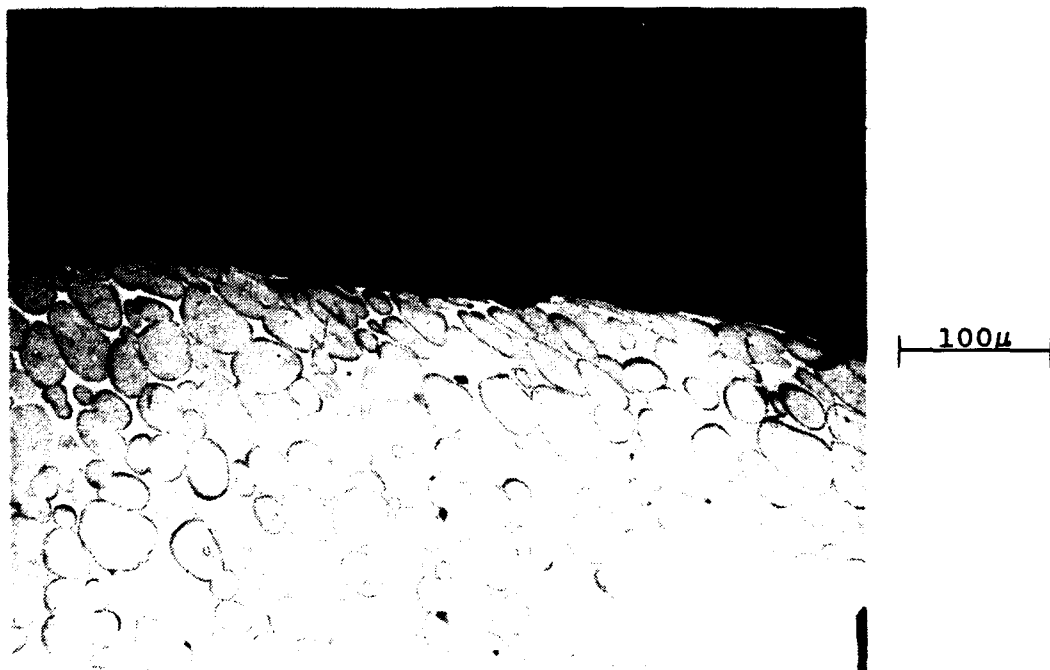
Figure 22.   Region of Maximum Shear, #72, LPS 90%W, 200x

Figure 23. Deformations in Ballistically Tested Fragment, 500x
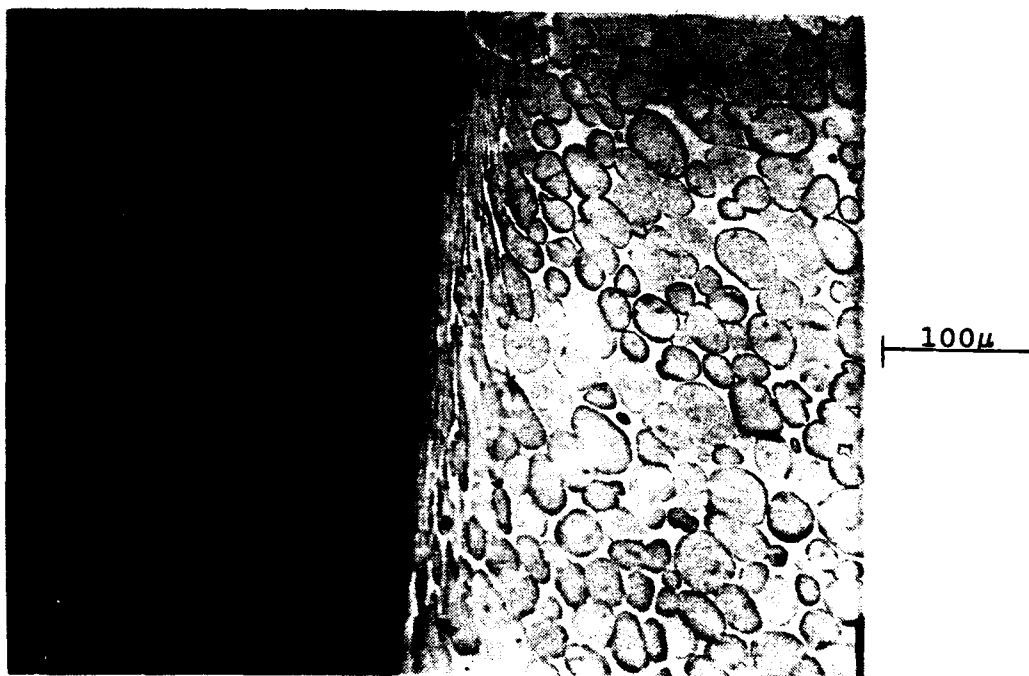
Figure 24. Region of Maximum Strain, #73, LPS 90%W, 200x

slightly different alloy and consequently has a greater grain size.

Sample 52 was tested using the same conditions as sample 49 except the punch had a flat face instead of a slanted face. Like sample 49, it was originally thought that it did not punch through, but metallographic examination revealed that it did indeed fail completely across the section. The tungsten grains here show greater ductility and deformation than those in sample 49 and the tungsten grain contacts appear stronger here, Figure 26. It may be possible that the flat punch applies more of a pure shear stress in the struck region than the slanted punch, which may be applying a superimposed shear and tensile stress.

4.3.2 Coated Tungsten Powder (CWP)

Sample 35, and all of the samples in this group, were consolidated by hot isostatic pressing (HIP). The appearance of the bulk microstructure is identical to the liquid phase sintered samples and suggests the samples were over-HIPed, Figure 27 . Properly consolidated coated tungsten powder should have tungsten particles completely surrounded by the matrix, effectively eliminating all tungsten-to-tungsten particle contacts, Figure 28 (Reference 9). The elimination of the tungsten grain contacts is expected to result in greater ductility and toughness. Preliminary results on transverse bend specimens has indicated that the strength is increased and the strain to failure is not degraded (Reference 9). Work with tensile specimens has indicated that the total matrix volume may be a significant factor in determining the final properties (Reference 20).

Sample 59 showed good ductility in the region of failure. The tungsten grains show moderate elongation but no overt signs of
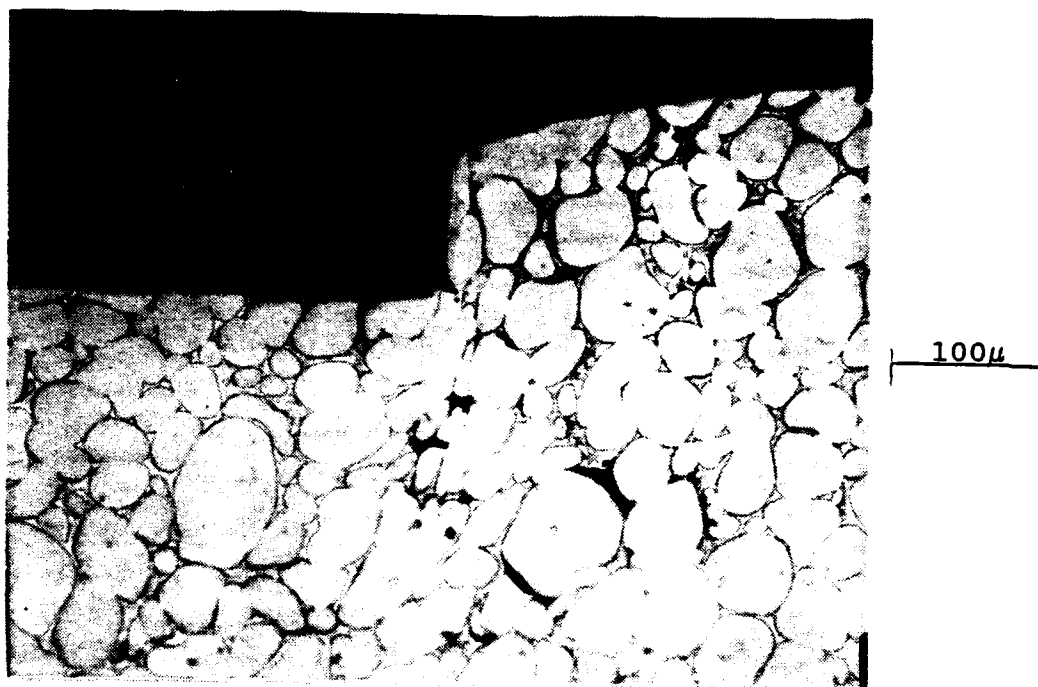
Figure 25.   Region of the Punch Strike, #71, LPS 90%W, 500°F

Figure 26.   #52 with Flat Punch - Compare with #49 with Slant Punch
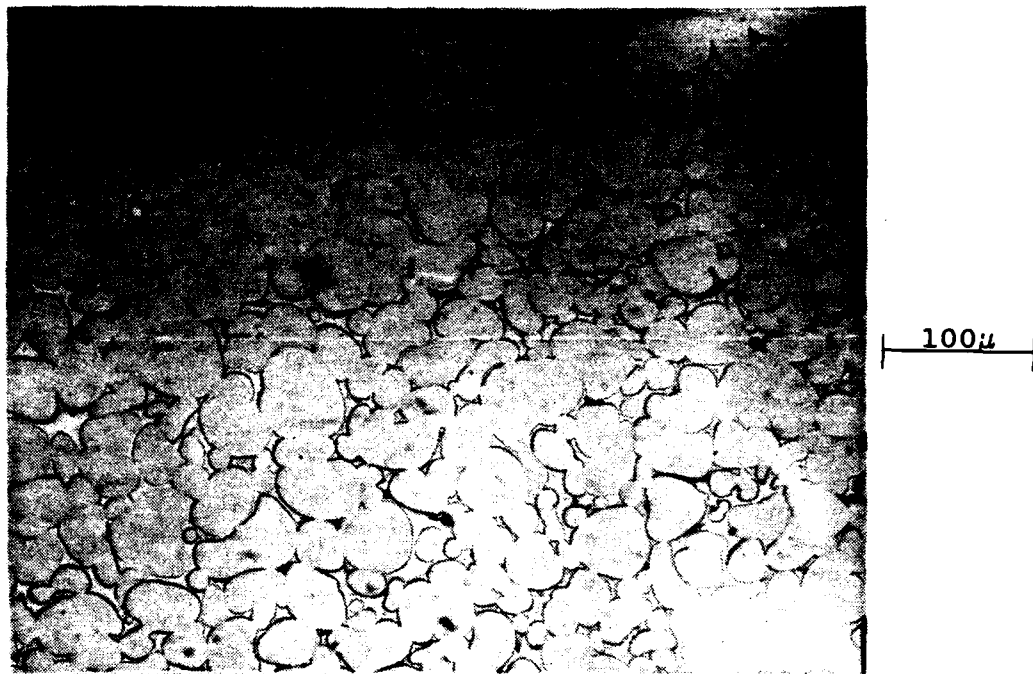
Figure 27.   Bulk Microstructure of CWP 95%W, #62, 200x
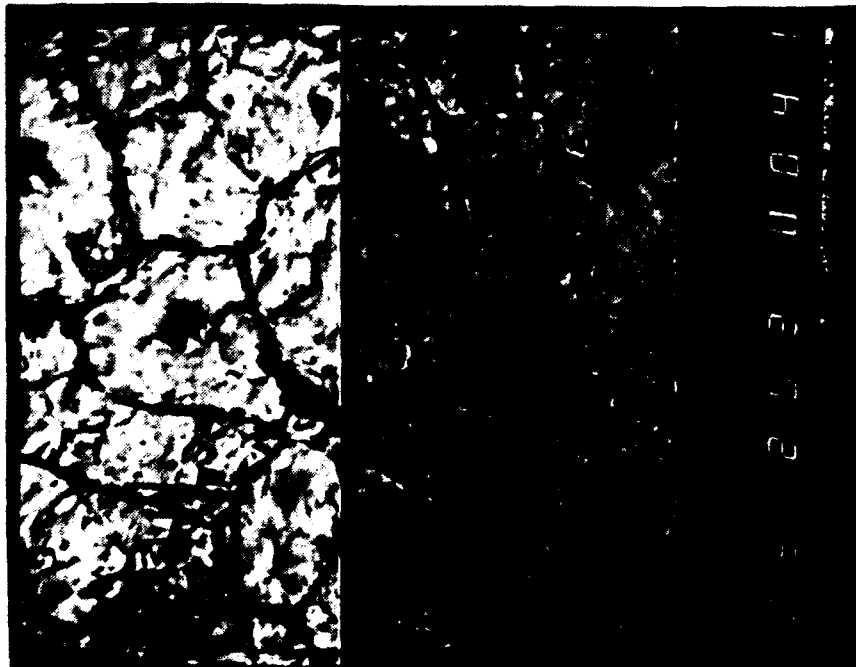
Figure 28.   Microstructure of Properly Consolidated Tungsten Powder

adiabatic shear localization, Figure 29.

Sample 62 showed much less ductility than either sample 35 or 59. This is seen in Figure 30, where the tungsten grains show no deformation and tungsten grain boundary failure is extensive. Compared to sample 71 (tested at the same conditions), sample 62 is much more brittle. It is likely a consequence of the greater tungsten content (and reduced matrix volume) of the coated powder samples that the ductility is less. Also, the greater the tungsten content, the greater the tungsten grain contact and a resultant decrease in the expected ductility.

4.3.3 Tungsten-Titanium Composites

Sample 44 (30 volume % titanium) failed in a completely brittle manner, showing no signs of localized shear behavior. Oxygen analysis of these samples (see Appendix A) indicates a very high content in all of the W-Ti samples. The titanium matrix of sample 44 is so brittle that cracks propagating through it avoid, and are blunted by, tungsten particles! This is shown in Figure 31.

Sample 53 (40 volume % titanium) behaved in a manner very similar to sample 44. The crack path avoided tungsten particles and the bulk microstructure. Figure 32 shows titanium grain boundaries decorated by oxide particles.

Sample 55 (50 volume % titanium) contained so much titanium that gravitational segregation was a severe problem. Figure 33 shows the layered nature of this sample. Figure 34 shows the result of testing this sample in the region just below the struck area. The region containing the tungsten cracked, while the
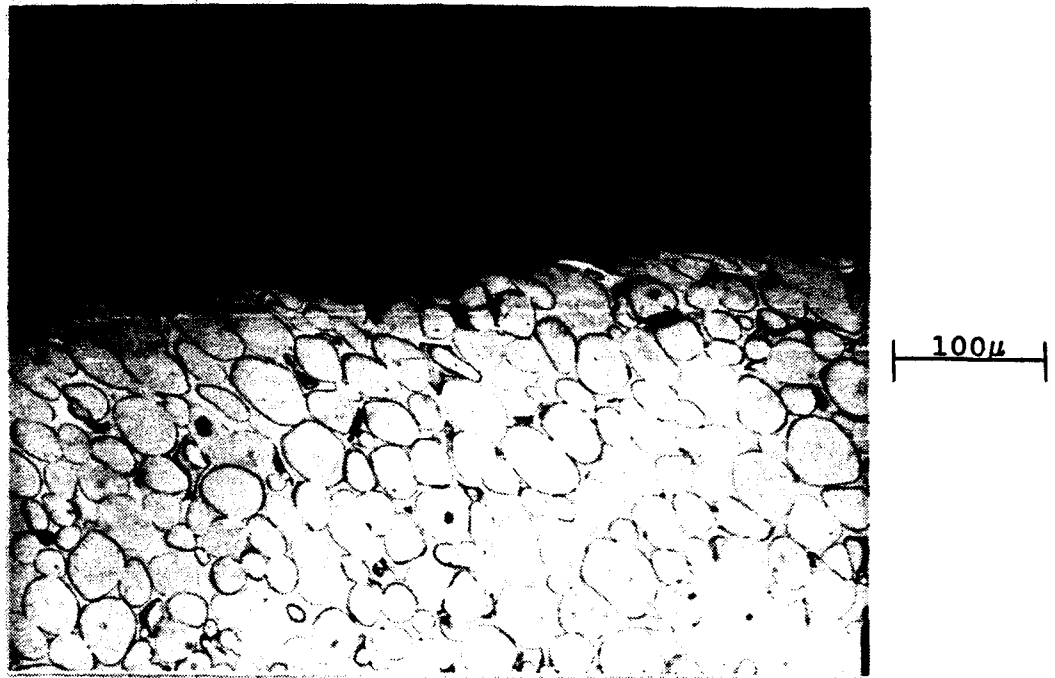
Figure 29.   Region of Failure of CWP 95%W, #59, Flat Punch, 530°F
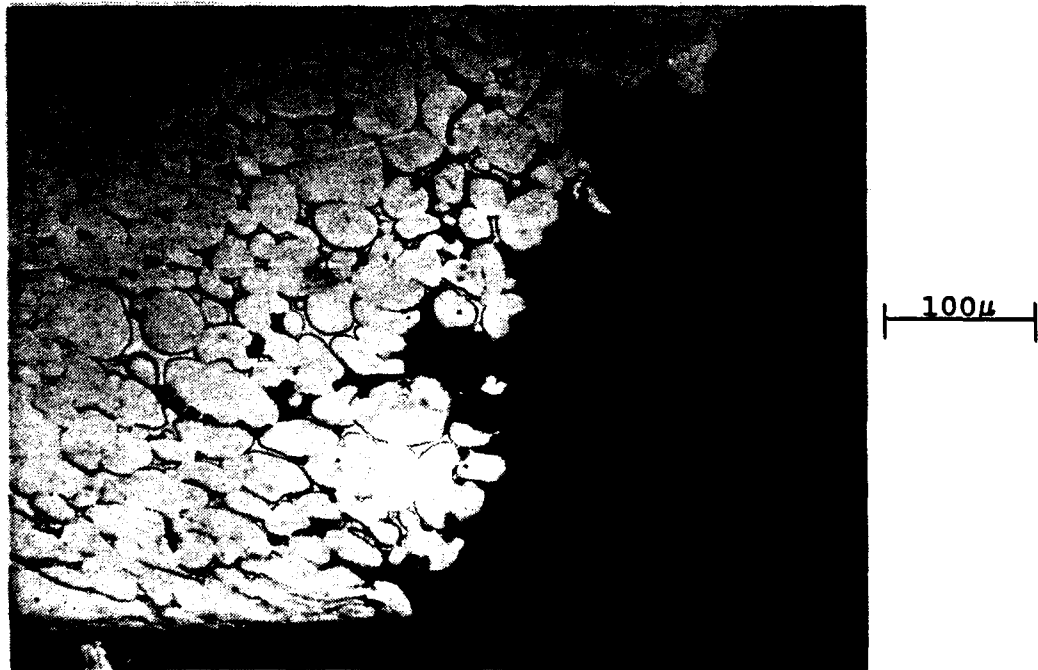
Figure 30.   Region of Failure of CWP 95%W, #62, Slant Punch, 550°F
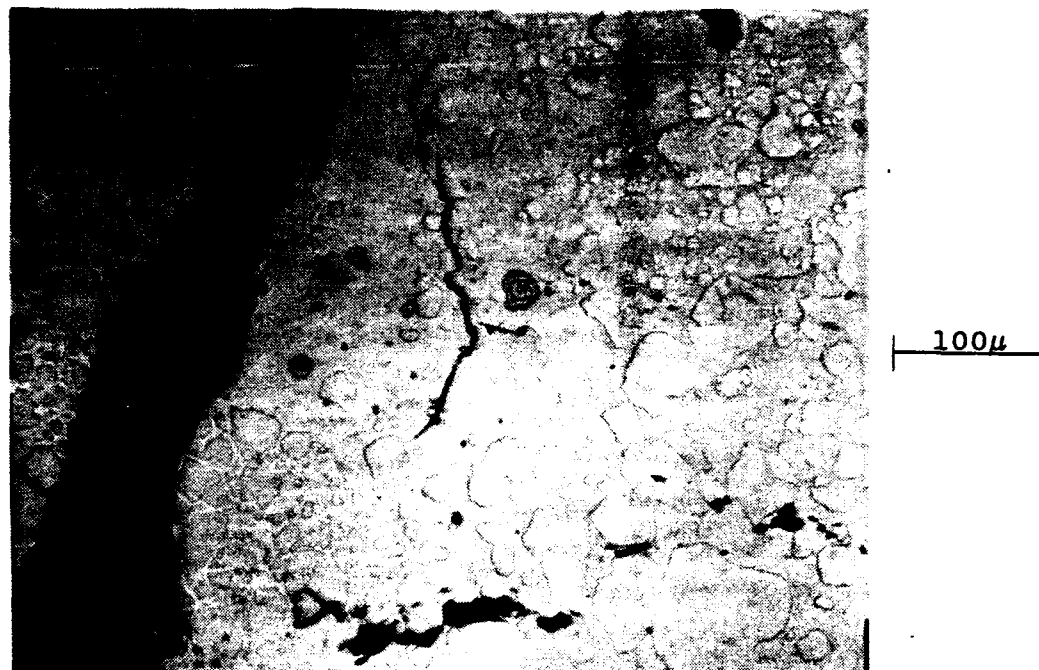
Figure 31. Region of Failure of W-30% Ti, #44, Flat Punch, Ambient
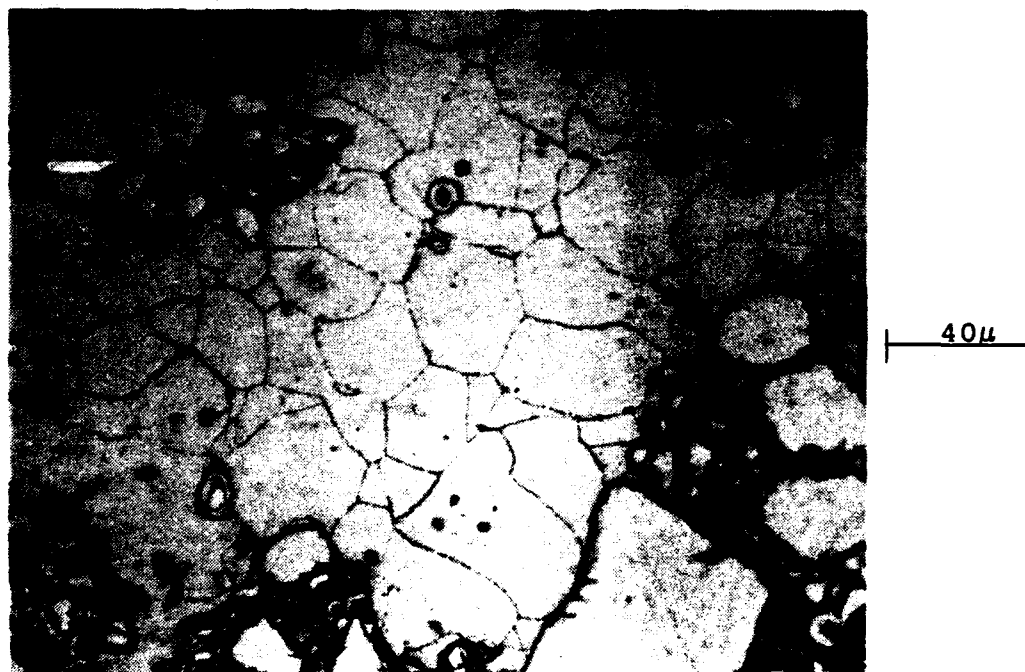
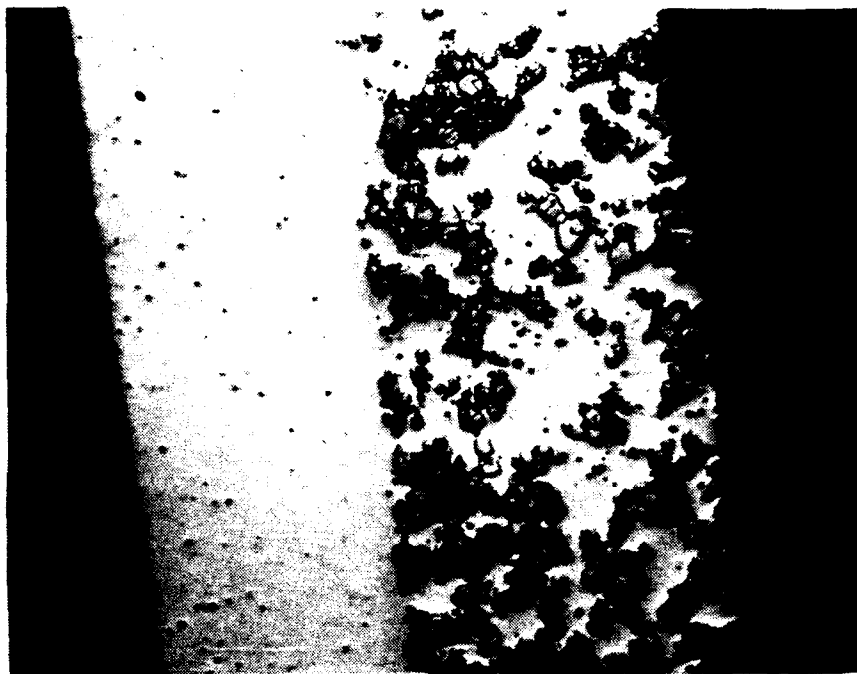Figure 32. Region of Failure of W-40% Ti, #53, Slant Punch, 280°F

Figure 33. Gravitational Segregation of W-50% Ti, #55

Figure 34. Region of Failure of W-50% Ti, #55, Slant Punch, 590°F

single-phase region displayed good tolerance for the impact. These samples had as much oxygen contamination as the other tungsten-titanium samples and seems to indicate that the tungsten may have been the source of the oxygen. It would seem likely that surface oxides on the tungsten powder contaminated the final product to the point that ductility was not available. Figure 35 shows cracking along the grain boundaries in this sample.

In all of the tungsten-titanium samples an interesting observation is that the titanium appears to have penetrated the grain boundaries of polycrystalline tungsten particles. This could have important implications for tungsten alloys in which the elimination of tungsten grain contiguity is an objective. This can be seen in many of the tungsten-titanium failures (Figures 31-35).

4.3.4 Tungsten-Zirconium Laminates

Sample 50 behaved in a brittle manner, similar to the W-Ti composites, but this sample did not suffer from the excessive oxygen content. The laminate nature of this sample is shown in Figure 36. The entire cross section was composed of approximately three lamination units. Figure 37 shows the crack path in the region of the punch strike. The crack clearly propagates through the tungsten phase, but there is no cracking in the zirconium layer. The original purpose of the zirconium was to provide a preferred crack path, but it certainly appears to not be the case.

Figure 35.   Cracking Along Grain Boundaries of #55, 500x
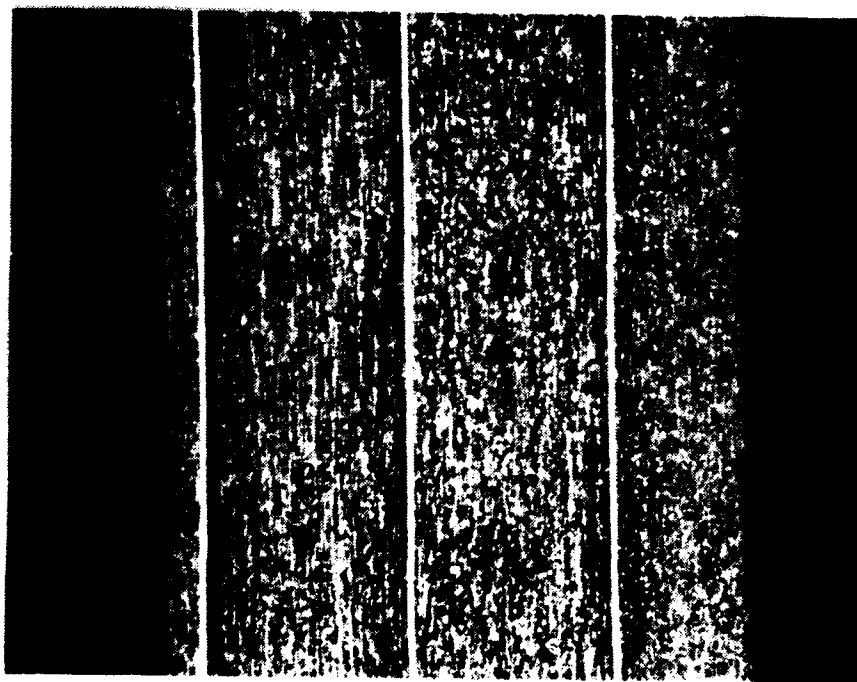
Figure 36.   Zr-W Laminations, Sample Number 50, 50x

40μ
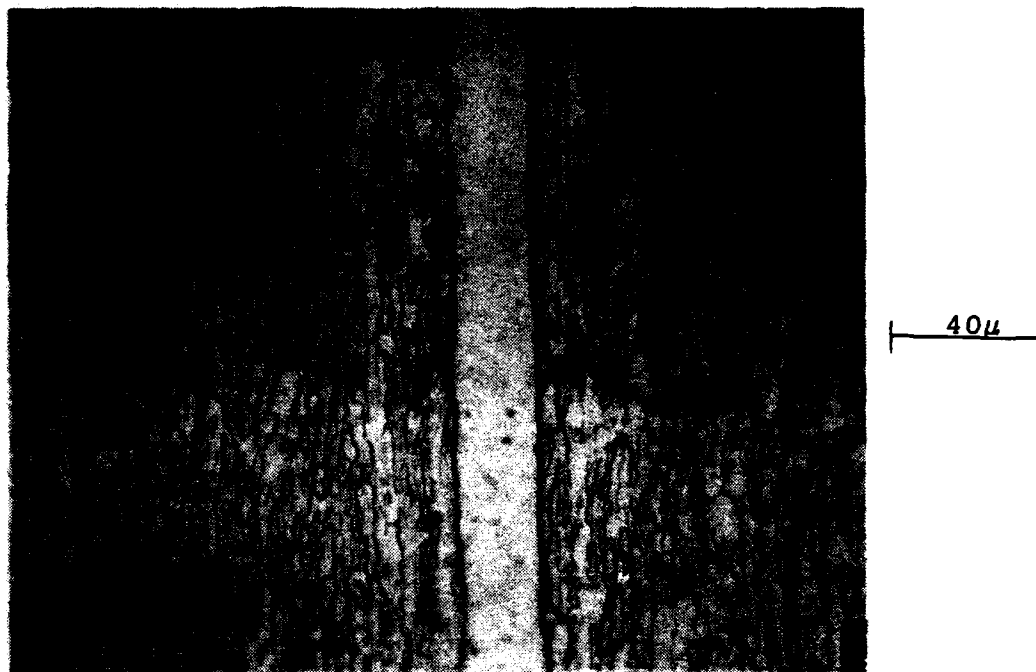
Figure 37. Crack Paths in Zr-W Laminations, Sample Number 50, 500x

5. CONCLUSIONS.

The conclusions that can be drawn from the metallographic examination of these tested samples can be summarized as follows:

(1) The liquid phase sintered 90% tungsten heavy alloy, supplied by GTE Products Corporation, was the only material that displayed room temperature ductility at all loading conditions.

(2) All of the samples consolidated by solid state means, i.e. HIP, did not display adequate ductility in room temperature testing.

(3) There were no samples examined that revealed any tendency toward adiabatic shear localization as evidenced by a lack of shear bands in the cross sectional microstructure.

(4) Oxygen contamination of the tungsten-titanium composite samples was the likely reason for the poor behavior of that group of samples. The oxygen was most likely introduced by the tungsten powder. Evidence supporting this statement can be found in examining the 50 volume percent sample in which gravitational segregation resulted in two distinct layers. The two-phase layer cracked, while the single-phase (titanium only) layer displayed good tolerance for the impact.

(5) The tungsten-zirconium laminates did not show the desired bahavior, i.e., localized failure along the Zr layer. One reason could have been the low number of laminations used to construct the structure. More and finer laminations may yet result in the sought for localization.

(6) Hot isostatic pressing of the coated tungsten powder at 1475 °C, liquid phase sintering under pressure, was inappropriate for this special powder. Solid state consolidation at a lower temperature was called for if preservation of the coating was to occur.

In addition to the metallographic conclusions stated above, approximate measurements of kinetic energy absorbed during the shear-punching process (Table 8) indicated the highest energy absorbed by LPS 90%W followed in decreasing order by CWP 95%W, Zr-W Laminate, and W-Ti compositions.

REFERENCES

1. Magness, L.S. and T.G. Farrand "Deformation Behavior and its Relationship to the Penetration Performance of High-Desity KE Penetrator Materials" U.S. Army Scientific Conference, 12-13 June 1990

2. Dowding, R.J. "Tungsten Alloy Research at the U.S. Army Materials Technology Laboratory" TMS Annual Mtg., New Orleans, LA, February 1991, Tungsten and Tungsten Alloys - Recent Advances, A. Crowson and E. Chen, Eds., 1991

3. Meyers, M.A. and L.E. Murr "Shock Waves and High-Strain-Rate Phenomena in Metals", Plenum Press (1981)

4. Kornhauser, M. "Design of 200,000G Shock Test Facility", 3C Systems Interim Report for Picatinny Arsenal, Contract No. DAAA21-85-C-0299, February 1986

5. Donnell, L.H. "Longitudinal Wave Transmission and Impact" APM-52-14, 153-166, 1930

6. Recht, R.F. " Analytical Modeling and Plate Penetration Dynamics" Chap. 7 in High Velocity Impact Dynamics" by J.A. Zukas, Ed., John Wiley & Sons, Inc., 1990

7. Kornhauser, M. "Structural Effects of Impact", Spartan Books, Inc., Cleaver-Hume Press, 1964

8. Spencer, J.R., "Relationship Between Composition, Structure, Properties, Thermomechanical Processing and Ballistic Performance of Tungsten Heavy Alloys", GTE Products Corporation, Final Report, U.S. Army Materials Technology Laboratory, Watertown, MA, July 1991.

9. Williams, B.E. et al, "CVD Coated Tungsten Powder Composites, Part I: Powder Processing and Characterization", Tungsten and Tungsten Alloys - Recent Advances, TMS, Warrendale, PA c1991.

10. Williams, B.E. et al, "CVD Coated Tungsten Powder Composites, Part II: Powder Fabrication and Properties", Tungsten and Tungsten Alloys - Recent Advances, TMS, Warrendale, PA c1991.

11. Mulligan, S. and R.J. Dowding," Sinterability of Tungsten Powder CVD Coated with Nickel and Iron", U.S. Army Materials Technology Laboratory, Watertown, MA, MTL TR 90-56, November 1990.

12. Bose, A. et al, "Test Temperature and Strain Rate Effects on the Properties of a Tungsten Heavy Alloy", Met Trans A, Vol. 19A, March 1988, p 487.

13. Yoon, H.K. et al, "Effect of Vacuum-Treatment on Mechanical Properties of W-Ni-Fe Heavy Alloy", J. Mat. Sc., Vol. 18, 1983, p 1374.

14. Churn, K.S. and D.N. Yoon, "Pore Formation and its Effect on Mechanical Properties in W-Ni-Fe Heavy Alloy", Powder Metall., 1979, p 175.

15. Churn, K.S. and R.M. German, "Fracture Behavior of W-Ni-Fe Heavy Alloys", Met Trans A, Vol. 15A, 1984, p 331.

16. Rabin, B.H. and R.M. German, "Microstructure Effects on Tensile Properties of Tungsten-Nickel-Iron Composites", Met Trans A, Vol. 19A, 1988, p 1523.

17. Ariel, E. et al, "Preparation and Properties of Heavy Metals", Powder Metall. Int'l, Vol. 5, No. 3, 1973, p 126.

18. Gerlach, U., "Microstructural Analysis of Residual Projectiles - A New Method to Explain Penetration Mechanisms", Met Trans A, Vol. 17A, 1986, p 435.

19. Tauer, K.J. and R.J. Dowding, Unpublished Research, 1991.

20. Dowding, R.J., Unpublished Research, 1991.

APPENDIX A

PREPARATION OF TUNGSTEN COMPOSITES
FOR HIGH STRAIN RATE TESTING

Dr. Peter E. Price

Preparation of Tungsten Composites for High Strain Rate Testing

To complement development of initial testing of an EHB facility to permit
high strain rate (shear) testing of potential new K.E. penetrator
materials, IMT prepared 1" diameter x .0625" thick test coupons of several
novel tungsten composites using hot isostatic pressing as the primary
process. With a view to the utilization of materials which might undergo
dynamic plastic flow instability due to adiabatic strain conditions caused
by "low" thermal diffusivity and high work of deformation (internal heat
generation) and/or dynamic localized temperature that rises to a level
where phase transformation plastic flow instability would be encountered,
three composites of W-Ti, a layered composite of W-Zr, and a composite of
CVD Fe-Ni were prepared. Details of the process and information on
structure and hardness follow below.

Materials

Five composite materials were prepared as listed in Table I.

Table I

Composite	Description and Materials Source
1. W/Fe, Ni (powder)	CVD coated W powder, 3.0 wt% Ni, 1.6 wt% Fe, Ultramet Lot #083190A, 902 gm supplied.
2. W/Zr laminate	Interleaved .021" thick W discs and .001" thick Zr foil. W: Schwarzkopf Dev. standard electrical contact discs, material certification – see appendix. Zr: Teledyne Wah Chang.
3. W/Ti 30 vol% (powder)	Blended elemental powders. W: General Electric Co. approximately 20 micron mean particle size, certification – see appendix. Ti: -325 mesh CP Ti sponge fines, Micron Metals, Inc.
4. W/Ti 40 vol% (powder)	Same as (3).
5. W/Ti 50 vol% (powder)	Same as (3).

Processing

Processing steps used for each composite are listed below.

Composite 1 - W/FeNi

1. Measure tap density = 10.41 g/cc approximately .54 theoretical density
2. Trial cold press powder 53 ksi .377 diameter x .286" high, approximately .70 theoretical density
3. Trial cold press 1 1/2" diameter x approximately 1 1/2" high minimum
   a. 30 tsi - no green strength
   b. 60 tsi - cracked compact
   c. 45 tsi - cracked compact; ρ = .64 theoretical
   Use 45 tsi compact for further processing.
4. Hydrogen sinter compact 3c above, 1300 C, 4 hrs, 1 atm hydrogen. ρ sinter approximately .78 ρ theoretical. Diameter pre-sinter = 1.515"; diameter post-sinter = 1.447".
5. Fabricate and vacuum anneal 1 1/2" ID x .065" wall x 2.4 " high HIP capsule.
6. Assemble, weld on cover, helium mass spectrometer leak check capsule and sintered W/FeNi compact.
7. Heat and evacuate capsule at 400°F, 2 hrs, crimp exit tube.
8. HIP: 6°C/min ramp to 1350°C, hold 1 hr; ramp to 1475°C, 1°C/min, hold 2 hrs, 15 ksi; furnace cool.
9. Decan machine.
10. Cut off and machine 1" diameter x .0625" discs for EHB test coupons.
11. Estimate ρ = 18.1g/cc.

Composite 2 - W/Zr Foil Laminate

1. Procure capsule components: 1 1/4" OD x .065" wall CP Ti tubing and machined CP end caps.
2. Procure 1" diameter x .020" thick W discs (electrical contact blanks from rolled sheet) from Schwarzkopf Development Corporation.
3. Cut 1+" diameter discs from .001" Zr foil stock (in house).
4. Hydrogen anneal W discs at 1200°C, 1 hr, white glove handling after anneal.
5. Clean Zr discs in acetone.
6. Assemble W/Zr stock 2.3" high and wrap with 4 1/2 layers of .045" Ti foil to maintain alignment and take up empty space in capsule.
7. Final weld assembly and then mass spectrometer leak check Ti capsule.
8. Warm outgas (400°F, 2 hrs) under vacuum and crimp capsule exit tube.
9. HIP at 1200°C, 2 hrs, 15 ksi. Ramp to 1200 C at 6°C/min. Furnace cool after 2 hr hold at temperature.
10. Decan machine.
11. Cut off and machine 1" diameter x .0625" discs. Note that positioning of Zr layers varied with respect to disc surfaces from disc to disc.

Composites 3, 4 & 5 - W/30, 40 and 50 vol% CP Ti

1. Procure and fabricate CP Ti capsule components. Ti tubing 1 1/2" OD x .065" wall x .044" wall thickness.
2. Weigh and blend (1 hr) 1000g of 30 vol% W/Ti powder to determine tap density and need for precompaction prior to encapsulation. Tap density is approximately 0.40 of theoretical. Precompaction deemed necessary.
3. Trial CIP (cold isostatic pressing) 50 vol% Ti composite at 28 ksi. ρ approximately .70 ρ theoretical.
4. Weigh and blend 30, 40 and 50 vol% Ti/W composite powders.
5. CIP cylindrical compacts of all three blends at 60 ksi.
6. Machine CIPed cylinders to 1.39" diameter for fit into Ti tube capsule.
7. Measure CIPed density.
   a. 30 vol% Ti/W
      ρ = 11.62 g/cc approximately .78 ρ theoretical
   b. 40 vol% Ti/W
      ρ = 10.64g/cc approximately .80 ρ theoretical
   c. 50 vol% Ti/W
      ρ = 9.88g/cc approximately .83 ρ theoretical
8. Load CIPed and machined PM slugs into Ti capsules, weld assemble and helium mass spectrometer leak check.
9. Warm outgas 400°F, 5 hrs under vacuum. Crimp exit tubes at 30μ.
10. HIP. Ramp 6 °C/min to 1350 °C, hold 1 hr at 15 ksi. Ramp 1 °C/min 1350 °C to 1450°C, hold 3 hrs at 1450 C, 15 ksi. Furnace cool.
11. Decan machine.
12. Machine 1" diameter x .0625" discs for EHB test coupons.

Properties, Structure and Chemistry

Hardness of the W/Ti composite material was determined after HIP and after several heat treatments aimed at reducing hardness and possibly increasing toughness. Results are summarized in Table II.

Table II
W/Ti PM Composite Hardness, R_c

Heat Treatment	30 vol% Ti (9.1 wt%)	40 vol% Ti (13.5 wt%)	50 vol% Ti (18.9 wt% Ti)
1. HIPed*	48.5	51.4	51.6
2. HIP + 700°C, 12 hrs, vacuum*	47.9	50.0	51.6
3. HIP + 740°C, 18 hrs, vacuum	47.7	50.1	51.0
4. HIP + 800°C, 12 hrs, vacuum	47.6	49.8	50.5

*Heat treated condition(s) supplied for EHB tests.

Examination of the accompanying annotated Ti-W phase diagram shows (assuming the diagram is correct) that in order to heat treat in the miscibility gap, at the eutectic temperature or in the alpha Ti/W field, heat treatment temperatures were all less than 0.5 Tm (homologous temperature for 40 vol% Ti) where a very slow kinetic response would be expected. Heat treatment produced only a very small change in hardness. SEM and TEM studies would be required to reveal low level microstructure changes. Density measurements were made on the discs machined from HIPed W/Ti PM material; Table III compares measured and theoretical density base on a rule of mixtures assuming no alloying effects.

Table III
Density, g/cc

	Theoretical	Measured
W/30 vol% Ti	14.8	15.0
W/40 vol% Ti	13.3	13.6
W/50 vol% Ti	11.9	12.1

Measured density greater than theoretical may relate to solid solution alloying effects, most likely W in solution in Ti. EDAX area scans would be required to establish the extent of alloying.

Microstructures of the five composite materials are shown in Figures 1-11. All composites appear fully dense.

The W/CVD Fe-Ni composite showed "pooling" of the Fe-Ni phase although a uniform initial particle coat has been assumed but not confirmed. There is little W particle rounding even though there is at least 20 wt% W solubility of W in Fe and Ni at 1450 C. There is some evidence of a remaining Fe-Ni film between W particles.

Laminated W/Zr showed a thin layer of a distinct composition as revealed by etching. This is expected to be W_2Zr (reference attached W/Zr phase diagram). Delamination was observed in cutting machining and EHB testing reflecting a brittle interface structure.

Wi/Ti PM composites were all HIPed in the beta (Ti,W) field of the W/Ti phase diagram. Solutioning of W would be expected at 1450°C and is supported by rounding of all W particles. It also appears that W particles, however close together, are separated by a Ti alloy layer. This suggests that Ti readily wets W under the applied process conditions and will diffuse to surround and separate the W particles. The uniformity of this behavior for all three composites further suggests that Ti volume

"fractions" in the 5-30% range might also, with proper process conditions, still provide a continuous bonding base. Composite densities would increase from 14.8 g/cc (30% theoretical) up to 18.6 g/cc (5% Ti). Process improvements could include selection of a "fine cut" of W powder, i.e., 1-5 microns mean particle size, hydrogen reduction to reduce oxygen level, CVD Ti coat on W powder, etc., all changes aimed at improved toughness combined with a potential for adiabatic shear deformation at high strain rate.

Presence of oxygen in both Ti and W alloy systems is known to reduce toughness. Oxygen in each of the machined disc composites was measured using a calibrated oxygen combustion (LECO) apparatus. Results are listed in Table IV.

<div align="center">

Table IV
Oxygen Content, PPM by wt.

</div>

Composite	Value (average of N readings)
1. W/3% Fe 1.6% Ni	5.4 (3)
2. W/Zr laminate	8.5 (2)
3. W/30 vol% Ti	315 (5)
4. W/40 vol% Ti	347 (3)
5. W/50 vol% Ti	408 (3)

A copy of original data is appended.

Mechanical Behavior

The rationale for running some EHB tests at elevated temperature comes from commercial literature applicable to the rolled W sheet used for disc lamellae in the W/Zr laminate: reference Fig. 12. For .0625" (1.5 min) W sheet, the ductile (brittle transition) temperature is approximately 250°C (482°F). Punching temperature recommended is approximately 550°C (1020°F) minimum. This exceeds the temperature used for heated specimens in EHB testing so that brittle behavior (assuming W fracture character is controlling in the composites) would still be expected. Shift away from brittle behavior was observed in several cases on the disc and residual "ring." This suggests that changes such as reduced grain size and reduced oxygen normally employed to increase toughness could be further exploited if toughness is functionally required for penetrator material.
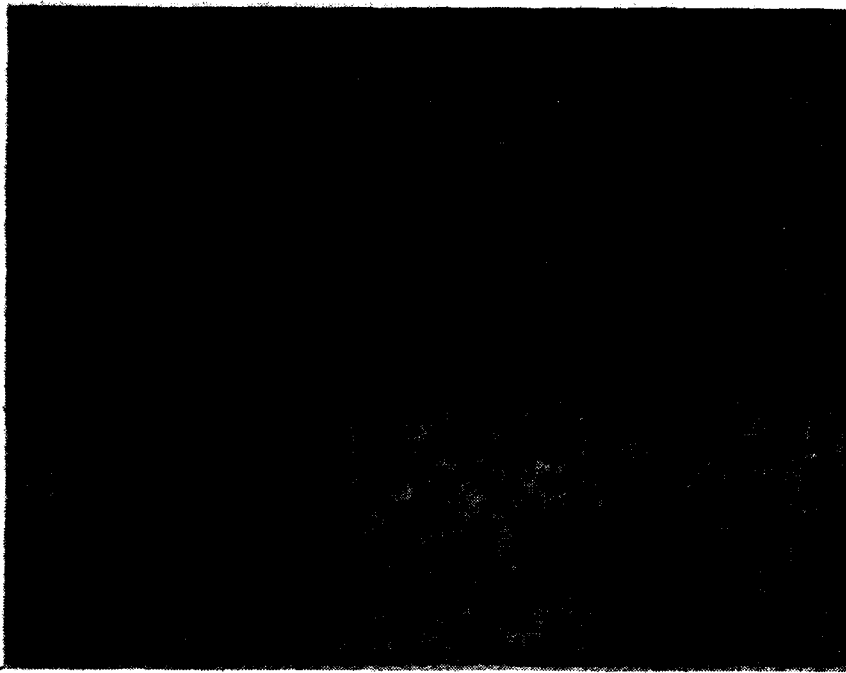
Fig. 1
W/3% Ni-1.6% Fe CVD, 100X
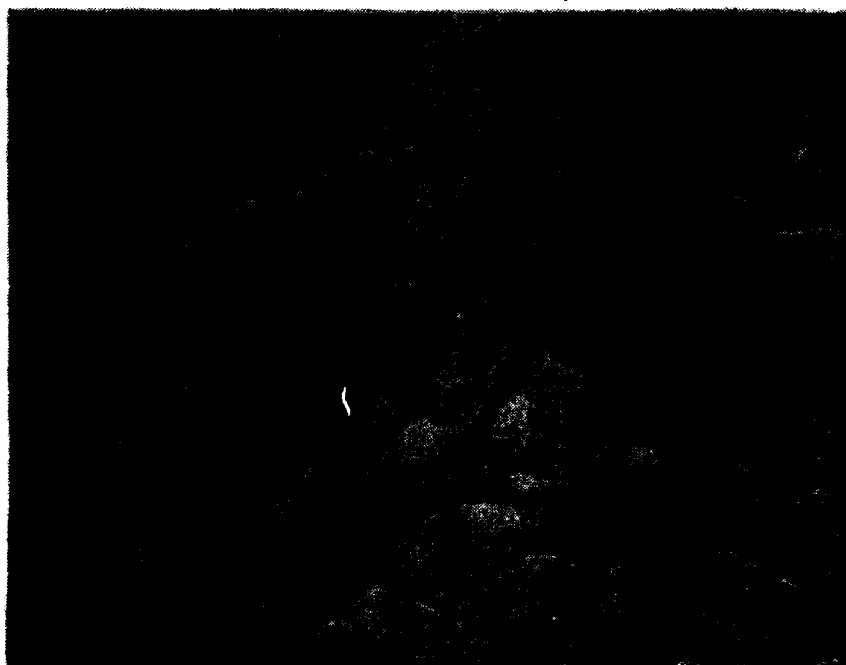
Fig. 2
W/Fe-Ni, 500X

Fig. 3
W/Zr laminate with cracking delamination, 50X
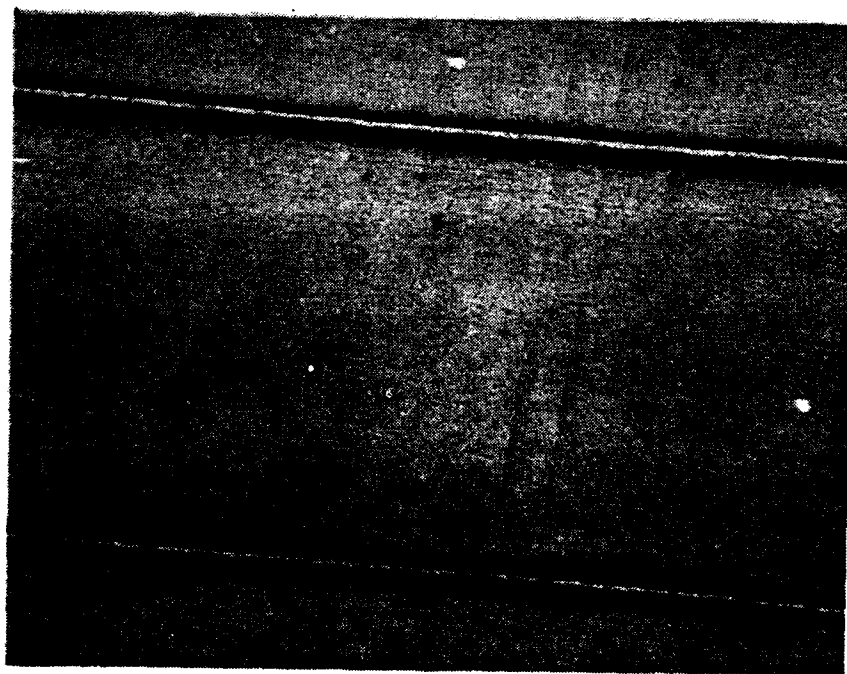
Fig. 4
W/Zr laminate, 100X

Fig. 5
W/Zr laminate, 500X
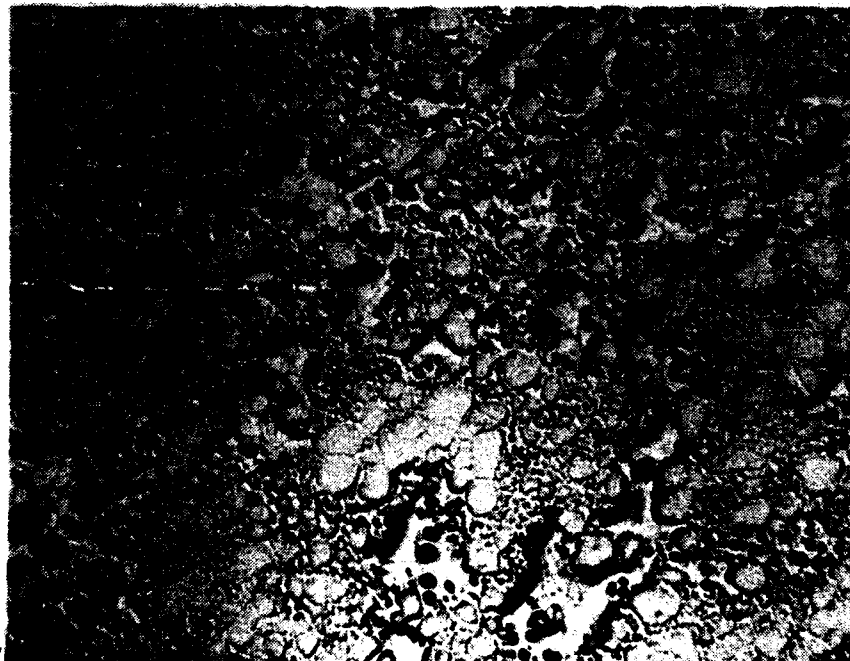
Fig. 6
W/30 vol% Ti, W particles, Ti network, 100X
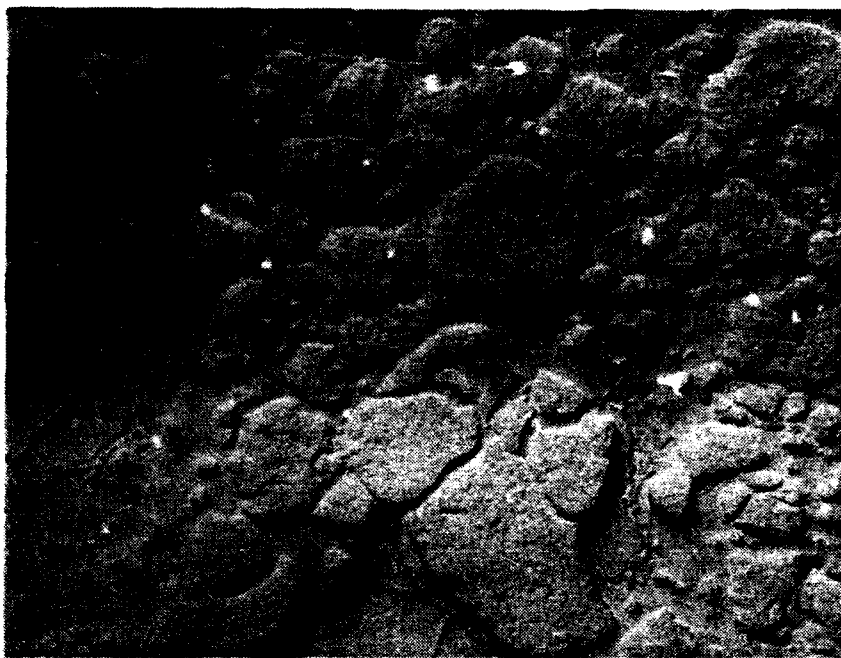
Fig. 7
W/30 vol% Ti, 500X
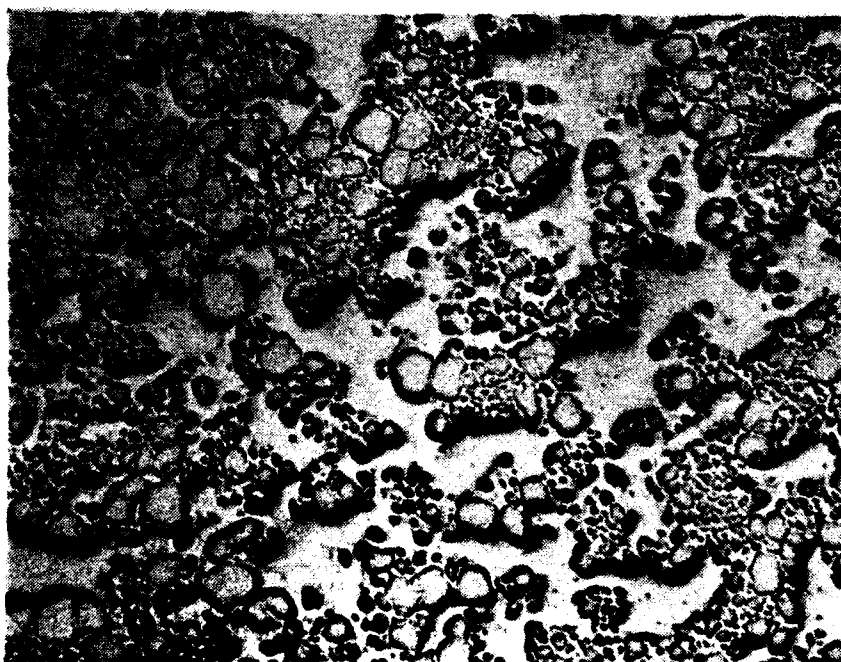
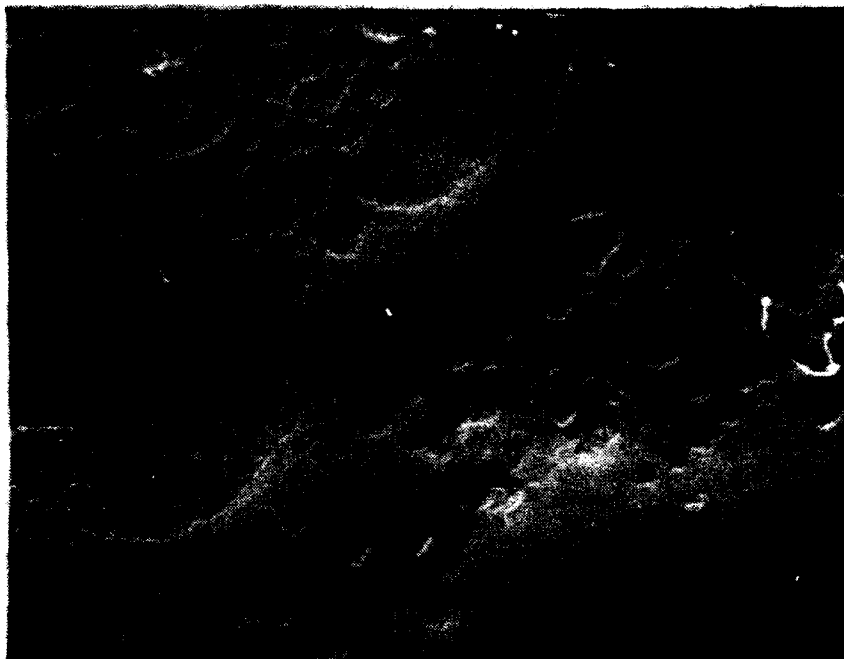
Fig. 8
W/40 vol% Ti, 100X

Fig. 9
W/40 vol% Ti. 500X
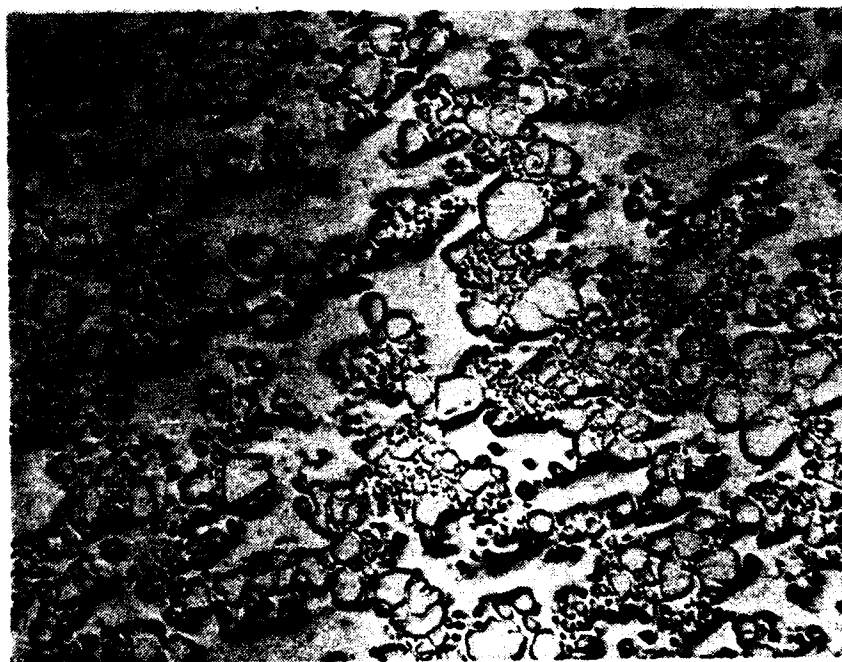
Fig. 10
W/50 vol% Ti. 100X

Fig. 11
W/50 vol% Ti, 500X

Spanlose Formgebung, Stanzen und Schneiden

Der Temperaturbereich für die Verarbeitung von Wolfram wird durch die Übergangstemperatur gegen tiefere Temperaturen, und durch die Rekristallisationstemperatur gegen hohe Temperaturen begrenzt.

In Abb. 15 sind empfohlene Temperaturbereiche für das Biegen und das Stanzen von Wolfram in Abhängigkeit von der Blechdicke wiedergegeben.

Dünne, stark verformte Bleche und Folien besitzen infolge der „Kornstreckung" durch das Walzen ausgeprägte Gefügestrukturen in Längsrichtung. Ihre Biegeeigenschaften längs und quer zur Walzrichtung sind daher verschieden. Wolframbleche sollten des-

Bending, Forming, Stamping, Punching and Cutting

The recommended temperature range for these operations is above the brittle-ductile transition temperature and below the recrystallization temperature. Fig. 15 shows the recommended temperature ranges for bending and punching of tungsten as a function of the sheet thickness.

Thin, intensely worked sheet and foil, due to the preferred orientation of the grains by rolling in the longitudinal direction, have pronounced longitudinal structures. Their bending properties, parallel and transverse to the rolling direction, differ considerably. Generally we recommend, that tungsten sheet is bent only transverse to the rolling direction, i.e. the longitudinal direction.

Déformation sans enlèvement de copeaux, cisaillage et découpage

Les températures pour l'usinage du tungstène sont limitées par la température de transition vers des températures plus basses, et par la température de récristallisation vers les températures élevées.

Figure 15 montre les températures recommandées pour le pliage et le cisaillage de tungstène en fonction de l'épaisseur de la tôle.

Les tôles et les feuilles minces, fortement écrouies, ont leurs structures dans le sens de la longueur, ceci, du fait de »l'étirage des grains« par laminage. Leurs propriétés de pliage suivant qu'elles sont longitudinales ou transver-

Fig. 12
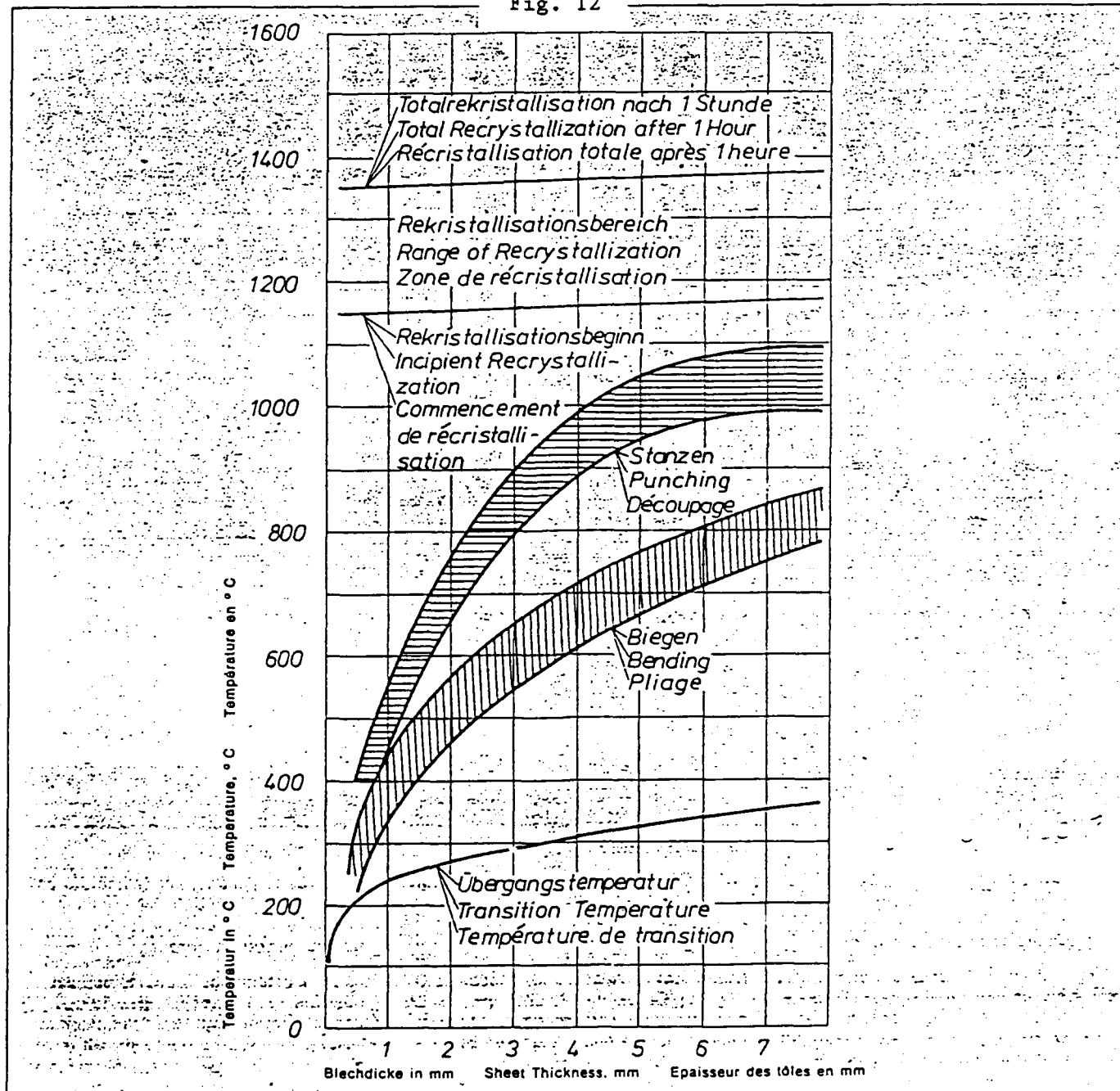
Abb. 15: Übergangstemperaturen, Rekristallisationstemperaturen und empfohlene Temperaturbereiche für das Biegen und Stanzen von Wolfram, o

Fig. 15: Transition temperature, recrystallization temperature and recommended temperature range for bend-ing and stamping of tungsten

– 74 –

Fig. 15 Temperature de transition, temperature de recristallisation et gamme de température recommancées

SCHWARZKOPF DEVELOPMENT CORPORATION

CUS.	ER'S ORDER NO.	DATE ENTERED 05/01/91	QUOTE NO. 5250	TERR. NO. 31	SALES ORDER NO. 4558-F		

ATTENTION:			215034		

	IMT - ANDOVER PO BOX 9569 155 RIVER STREET ANDOVER, MA 01810	DATE 05/16/91	CASE NO.	DATE SHIPPED

SOLD TO

PAGE 1

SHIP TO

INDUSTRIAL MATERIAL TECH
155 RIVER STREET
ANDOVER, MA 01810

REFER INQUIRIES TO
D. WHEELER

NET 30 DAYS

CERTIFICATION OF MATERIAL

The TUNGSTEN products contained in this shipment conform to

AMS 7897 _____
AMS 7898 _____

The composition of these products conform to the following analysis:

W	99.95%	Ag	5 PPM Max.	Mg	5 PPM Max.
C	30 PPM Max.	Al	10 PPM Max.	Mn	5 PPM Max.
O	30 PPM Max.	As	10 PPM Max.	Mo	300 PPM Max.
H	10 PPM Max.	Ba	10 PPM Max.	Nb	5 PPM Max.
N	10 PPM Max.	Cd	5 PPM Max.	Ni	20 PPM Max.
S	5 PPM Max.	Co	30 PPM Max.	Pb	10 PPM Max.
P	50 PPM Max.	Cr	10 PPM Max.	Ta	20 PPM Max.
Si	30 PPM Max.	Cu	20 PPM Max.	Ti	20 PPM Max.
Ca	30 PPM Max.	Fe	50 PPM Max.	Zr	20 PPM Max.
Zn	10 PPM Max.				

The MOLYBDENUM products contained in this shipment conform to

ASTM B384-74 Type 361 _____
ASTM B385-74 Type 361 _____
ASTM B386-85 Type 361 _____
ASTM B387-85 Type 361 _____

The composition of these products conform to the following analysis:

MO	99.95%	Ag	5 PPM Max.	Fe	100 PPM Max.
C	30 PPM Max.	Al	20 PPM Max.	K	10 PPM Max.
O	50 PPM Max.	As	10 PPM Max.	Mg	10 PPM Max.
H	10 PPM Max.	Ba	10 PPM Max.	Mn	5 PPM Max.
N	10 PPM Max.	Ca	20 PPM Max.	Na	10 PPM Max.
S	20 PPM Max.	Co	30 PPM Max.	Ni	10 PPM Max.
P	20 PPM Max.	Cr	20 PPM Max.	Pb	10 PPM Max.
Si	30 PPM Max.	Cu	30 PPM Max.	Ti	10 PPM Max.
				W	300 PPM Max.

- 75 -

Very truly yours,

SCHWARZKOPF DEVELOPMENT CC

GENERAL ⊛ ELECTRIC

21800 TUNGSTEN ROAD
CLEVELAND. OHIO 44117

COMPONENTS AND QUARTZ PRODUCTS DEPARTMENT

DATE: 6-11-91

TUNGSTEN POWDER LOT CERTIFICATION

Customer	Customer Order #	Lot #
INDUSTRIAL MATERIALS TECH. P.O. BOX 9565 155 RIVER ST. ANDOVER, MA 01810	21390	U16.5-7675
	Quantity Shipped	Date Shipped
	15.000 Kgs	6/13/91

AVERAGE PARTICLE DIAMETER BY FISHER SUB-SIEVE SIZER

Powder Condition	As Supplied	Lab Milled
A.P.D. (microns)	19.91	17.36
Porosity Value	.575	.424

PARTICLE SIZE DISTRIBUTION BY TURBIDIMETRIC SEDIMENTATION

POWDER CONDITION   LAB MILLED
DISPERSION METHOD   ULTRASONIC

Micron Range	Weight Percent
0-1	
1-2	
2-3	
3-4	
4-5	
5-6	
6-7	TOO
7-8	COARSE
8-9	
9-10	
10-11	
11-12	
12-13	
13-14	
14-15	
15-20	
20-25	

CHEMICAL ANALYSIS FOR IMPURITIES

ELEMENT	PPM	ELEMENT	PPM
Al	< 2	Mg	< 2
Ca	8	Sn	< 2
Si	< 5	O	230
Mo	267	Na	22
Fe	23	K	6
Cr	8	Nb	< 20
Ni	19		
Cu	< 2		
Mn	3	W 99.9% min	

(By differences & on gas free basis.)

Apparent Density by Scott Volumeter
104.2 gm/cu/in.

The data shown have been determined in GE laboratories under standard conditions according to sampling and analytical techniques which we believe to be most reliable. Appropriate ASTM methods are used where applicable as specified in GE General Catalog 2A (00-90)85/3000.

Signed

W. G. Joles

W.G. Joles
Quality Specialist 7641

micron
METALS, INC.

TELECOPIER COVER SHEET

DATE: 5-14-91   (500) 475-2951

PLS DELIVER TO: Johnathan Saber

COMPANY: IMT

LOCATION:

FROM:

micron
METALS, INC.

ROBERT K. FRY
President

7186 West Gates Avenue
Salt Lake City, Utah 84120
(801) 250-5919
FAX (801) 250-7295

"Creative Solutions in Powdered Metals"

NO. OF PAGES TO FOLLOW: 0

COMMENTS: Re: Your Inquiry Tipowder

Ref: Your Telecon of 5-13-91 with our MW Stockes

Thank you for the inquiry!

Micron Metals is pleased to offer the following quotation:

Size/Grade: -325 mesh Ti-000 Ti powder

Quantity: 100 LBS

Price: $ 19.00/LB *

Delivery: Ex stock

* Price is quoted F.O.B. Salt Lake City, UT.
This Grade contains minimum purity of 99.4%.
Please call if you have any questions. Regards,

W-Zr Phase Diagram

Weight Percent Zirconium

Atomic Percent Zirconium

From [Zirconium].

Weight Percent Tungsten

L

(βTi,W)

1670°C

1250°C

882°C

740 ± 20°C

(αTi)

Ti

Atomic Percent Tungsten

W

3422°C

Atomic Percent Tungsten

L

(βTi,W)

1670°C

1250°C

882°C

740 ± 20°C

(αTi)

Ti

Weight Percent Tungsten

W

3422°C

2350
2150
2000±0.5 T_m
(2057°C)
1700

850
900
730

J.L. Murray, 1981.

JOB #   D-370

DATE   10/8/91

CALCULATED BY   J. LaGou

OXYGEN ANALYSIS RESULTS

W-3%, Ni-1.6%, Fe		W w/ Zr foil		W-30% Ti	
	%		%		%
0.00008	%	0.00151	%	0.03250	%
0.00101	%	6.00019	%	0.03384	%
0.00054	%		%	0.02664	%
	%		%	0.03300	%
Avg: 0.00054	%	Avg: 0.00085	%	Avg: 0.03150	%

W-40% Ti		W-50% Ti			
	%		%		%
0.03594	%	0.04062	%		%
0.03537	%	0.03943	%		%
0.03295	%	0.04251	%		%
	%		%		%
Avg: 0.03475	%	Avg: 0.04085	%	Avg:	%

Distribution List

1 Office of the Secretary of Defense for Research and
Engineering, The Pentagon, Washington, D.C. 20301

Commander, U.S. Army Laboratory Command, 2800 Powder Mill Road,
Adelphi, MD 20783-1145
1 ATTN: AMSLC-IM-TL
1 ATTN: AMSLC-CT

Commander, Defense Technical Information Center, Cameron Station,
Building 5, 5010 Duke Street, Alexandria, VA 22304-6145
2 DTIC-FDAC

1 MIAC/CINDAS, Purdue University, 2595 Yeager Road, West
Lafayette, IN 47905

Commander, Army Research Office, P.O. Box 12211, Research
Triangle Park, NC
     27709-2211
1 ATTN: Information Processing Office
1   Dr. Andrew Crowson
           Dr. Edward Chen

Commander U.S. Army Materiel Command (AMC), 5001 Eisenhower
Avenue, Alexandria, VA 22333
1 ATTN: AMCSCI

Commander, U.S. Army Materiel Systems Analysis Activity, Aberdeen
Proving Ground, MD 21005
1 ATTN: AMXSY-MP, Director

Commander, U.S. Army Missile Command, Redstone Scientific
Information Center, Redstone Arsenal, AL 35898-5241
1 ATTN: AMSMI-RD-CS-R/Doc

Commander, U.S. Army Armament Research Development and
Engineering Center,   Dover, NJ 07801
1 ATTN: Technical Library
1   Mr. D. Kapoor
1   Dr. S. Cytron

Commander, U.S. Army Tank-Automotive Command, Warren, MI
48397-5000
2 ATTN: AMSTA-TSL Technical Library

Commander, U.S. Army Foreign Science and Technology Center, 220
7th Street, N.E., Charlottesville, VA 22901
3 ATTN: AIFRTC, Applied Technologies Branch, Gerald Schlesinger

Naval Research Laboratory, Washington, D.C.   20375
1 ATTN: Code 5830
1   Code 2627

Chief of Naval Research, Arlington, VA   22217
1 ATTN: Code 471

Naval Surface Weapons Center, Dahlgren Laboratory, Dahlgren, VA
22448
1 ATTN: Code G-32, Ammunition Branch, Mr. Brian Sabourin

Commander, Rock Island Arsenal, Rock Island, IL   61299-6000
1 ATTN: SMCRI-SEM-T

Battelle Columbus Laboratories, Battelle Memorial Institute, 505
King Avenue, Columbus, OH   43201
1 ATTN: Mr. Henry Cialone
1   Dr. Alan Clauer

Battelle Pacific Northwest Laboratories, P.O. Box 999, Richland,
WA 99352
1 ATTN: Mr. William Gurwell
1   Dr. Gordon Dudder

GTE Sylvania, Inc. Chemical and Metallurgical Division, Hawes
Street, Towanda, PA 18848
1 ATTN: Dr. James Mullendore
1   Mr. James Spencer

Director, Ballistic Research Laboratory, Aberdeen Proving Ground,
MD   21005
1 ATTN: SLCBR-TSB-S (STINFO)
1   SLCBR-TB-P, Mr. Lee Magness

Teledyne Firth Sterling, 1 Teledyne Place, LaVergne, TN 37086
1 ATTN: Dr. Steven Caldwell
1   Dr. Thomas Penrice

Technology Associates Corp., 17911 Sampson Lane, Huntington
Beach, CA
    92647
1 ATTN: Dr. Gary Allen

Los Alamos National Laboratory, ATAC, MS F681, P.O. Box 1663, Los
Alamos, NM   87545
1 ATTN: Dr. Bill Hogan

Philips Elmet, 1560 Lisbon Road, Lewiston, ME   04240
1 ATTN: Mr. James Anderson

Ultramet, Inc., 12173 Montague Street, Pacoima, CA   91331
1 ATTN: Dr. J.J. Stiglich
1   Mr. Brian Williams
1   Dr. Robert Tuffias

Ceracon, Inc., 1101 N. Market Boulevard, Suite 9, Sacramento, CA 95834
1 ATTN: Dr. Ramas Raman

Southwest Research Institute, 6220 Culebra Road, P.O. Drawer 28510, San Antonio, TX 78228-0510
1 ATTN: Dr. Animesh Bose
1   Dr. James Lankford

Metalworking Technology, Inc., 1450 Scalp Avenue, Johnstown, PA 15904
1 ATTN: Mr. C. Buck Skena
1   Mr. Timothy McCabe

Research Triangle Institute, P.O. Box 12194, Research Triangle Park, NC 27709-2154
1 ATTN: Dr. John B. Posthill

3C Systems, 620 Arglye Road, Wynnewood, PA 19096
1 ATTN: Mr. Murray Kornhauser

Advance Technology Coatings, 300 Blue Smoke Ct. West, Fort Worth, TX 76105
1 ATTN: Mr. Grady Sheek

Alliant Techsystems, 7225 Northland Drive, Brooklyn Park, MN 55428
1 ATTN: Dr. Stan Nelson
1   Mr. MArk Jones
1   Mr. Thomas Steigauf

CAMDEC, 3002 Dow Avenue, Suite 110, Tustin, CA 92680
1 ATTN: Dr. Richard Harlow

Chamberlain Manufacturing Co., 550 Esther St., P.O. Box 2545, Waterloo, IA
    50704
1 ATTN: Mr. Tom Lynch

Defense Technology International, Inc., The Stark House, 22 Concord Street,
    Nashua, NH
1 ATTN: Mr. Douglas Ayer

Materials and Electrochemical Research Corporation, 7960 S. Kolb Road, Tucson, AZ 85706
1 ATTN: Dr. James Withers
1   Dr. Sumit Guha

Materials Modification, Inc., P.O. Box 4817, Falls Church, Va 22044
1 ATTN: Dr. T.S. Sudarshan

Micro Materials Technology, 120-D Research Drive, Milford, CT
06460
1 ATTN: Dr. Richard Cheney

Nuclear Metals, 2229 Main Street, Concord, MA 01742
1 ATTN: Dr. Willian Nachtrab

Olin Ordnance, 10101 9th Street N., St. Petersburg, FL
1 ATTN: Hugh McElroy

The Pennsylvania State University, Department of Engineering
Science and Mechanics, 227 Hammond Building, University Park, PA
16802-1401
1 ATTN: Dr. Randall M. German, Professor, Brush Chair in
Materials

Director, U.S. Army Materials Technology Laboratory, Watertown,
MA 02172-0001
2 ATTN: SLCMT-TML
1   SLCMT-IMA-V
1   SLCMT-PRC
20   SLCMT-MEM, Mr. Robert Dowding

AD _____

UNCLASSIFIED
UNLIMITED DISTRIBUTION

Key Words

Tungsten alloys
Tungsten composites
Dynamic tests

U.S. Army Materials Technology Laboratory,
Watertown, Massachusetts 02172-0001
DEVELOPMENT OF TUNGSTEN BASED COMPOSITES -
Murray Kornhauser
3C Systems, Inc., 620 Argyle Road
Wynnewood, PA 19096
Robert J. Dowding
U.S. Army Materials Technology Laboratory

Technical Report MTL TR 92-7, February 1992, 86 pp -
illus-tables, Contract DAAL04-91-C-0012
Final Report, February 1991 - October 1991

The objectives of this Phase I SBIR Program were to develop the test facility for very high strain rate shear testing of composite tungsten materials for use in kinetic energy (KE) penetrators, to test some composites prepared by liquid phase sintering and by the HIP process, and to determine whether the test samples exhibit evidence of favorable KE properties. An electromagnetic stress wave generator, with its output augmented with a conical Hopkinson bar, was used to drive a half-inch diameter punch through tungsten composite samples 1/16 inch thick and one-inch diameter. Initial strain rate on impact was up to 2.4×10^7 sec^{-1}, decreasing as the punch was decelerated by the test sample's resistance. Metallographic examinations were made; however, it is too early to report on promising trends. Phase II would include penetrator performance testing on target.